Siderophore-mediated iron enrichment in the biofilm matrix enhances plant iron nutrition

Tan, T.; Xu, Z.; Tao, L.; Sun, X.; Xie, J.; Miao, Y.; ... ; Shen, Q.

Cell Reports

Article

Siderophore-mediated iron enrichment in the biofilm matrix enhances plant iron nutrition

Graphical abstract

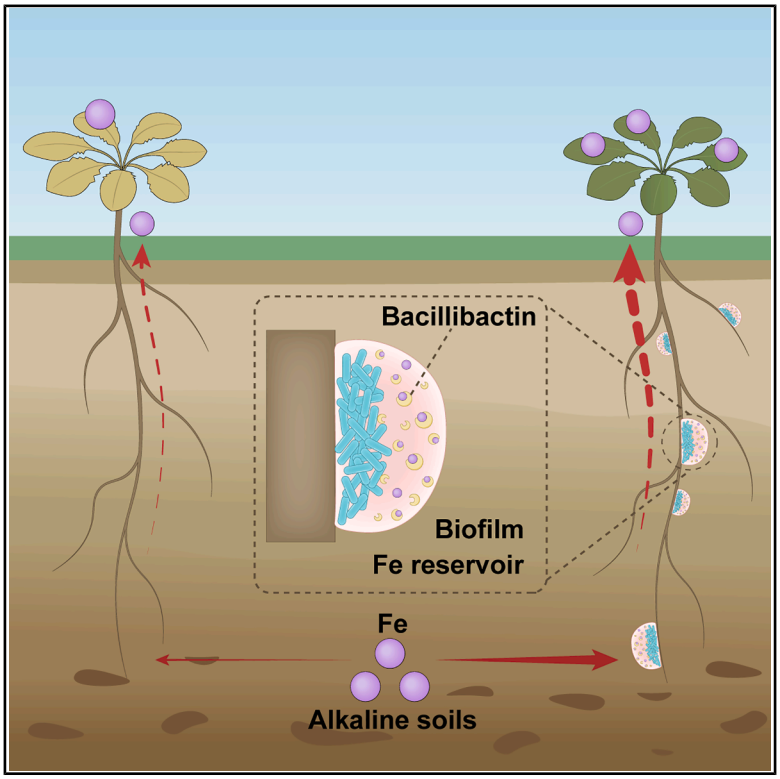

Highlights

- *B. velezensis* SQR9 biofilms accumulate Fe on plant roots and act as an Fe reservoir
- Plant roots colonized by SQR9 activated iron deficiency responses via siderophore
- Bacillibactin contributes to Fe accumulation in biofilms and activates root Fe uptake
- Application of SQR9 greatly boosted crop yields in alkaline soils in field trials

Authors

Taimeng Tan, Zhihui Xu, Lili Tao, ..., Wei Ran, Ruifu Zhang, Qirong Shen

Correspondence

xzh2068@njau.edu.cn (Z.X.), shenqirong@njau.edu.cn (Q.S.)

In brief

Tan et al. reveal that *Bacillus velezensis* biofilms accumulate Fe on roots, serving as Fe reservoirs to make Fe more accessible to the host plant. The bacterial siderophore bacillibactin plays a dual role by promoting Fe accumulation in the biofilms and activating plant Fe-deficiency responses.

Tan et al., 2025, Cell Reports *44*, 116481
November 25, 2025
https://doi.org/10.1016/j.celrep.2025.116481

CellPress

Cell Reports

CellPress
OPEN ACCESS

Article

Siderophore-mediated iron enrichment in the biofilm matrix enhances plant iron nutrition

Taimeng Tan,[1,5] Zhihui Xu,[1,5,*] Lili Tao,[1] Xinli Sun,[1] Jiyu Xie,[1] Youzhi Miao,[1] Nan Zhang,[1] Weibing Xun,[1] Pascale B. Beauregard,[2] Ákos T. Kovács,[3] Yifa Yu,[4] Yuan Luo,[4] Wei Ran,[1] Ruifu Zhang,[1] and Qirong Shen[1,6,*]

[1]Jiangsu Provincial Key Lab of Solid Organic Waste Utilization, Jiangsu Collaborative Innovation Center of Solid Organic Wastes, Jiangsu Provincial Key Laboratory of Coastal Saline Soil Resources Utilization and Ecological Conservation, Educational Ministry Engineering Center of Resource-Saving Fertilizers, Nanjing Agricultural University, Nanjing, Jiangsu 210095, P.R. China

[2]Département de Biologie, Université de Sherbrooke, Sherbrooke, QC J1K 2R1, Canada

[3]Institute of Biology, Leiden University, 2333 BE Leiden, the Netherlands

[4]Nanning Harworld Bio-technology Co., Ltd., Laboratory of Microbial Fertilizer, Ministry of Agriculture and Rural Affairs, Nanning, Guangxi 530000, P.R. China

[5]These authors contributed equally

[6]Lead contact

*Correspondence: xzh2068@njau.edu.cn (Z.X.), shenqirong@njau.edu.cn (Q.S.)

https://doi.org/10.1016/j.celrep.2025.116481

SUMMARY

Plant-beneficial microorganisms are frequently reported to enhance iron (Fe) nutrition in plants, yet the precise underlying mechanisms remain largely unknown. Although both bacterial siderophore production and biofilm formation are beneficial for microbial plant growth promotion, these two bacterial traits have been studied separately. Here, we reveal a strong coupling between these two bacterial traits in enhancing plant Fe uptake using the biofilm-forming rhizobacterium *Bacillus velezensis* SQR9. We demonstrate that SQR9 biofilms accumulate Fe on plant roots and serve as an Fe reservoir. Crucially, the siderophore bacillibactin enables biofilm Fe accumulation from the environment, while simultaneously stimulating Fe acquisition mechanisms in plants. Field experiments confirmed the ability of SQR9 to boost crop yields in alkaline soils, highlighting its potential for improving iron-limiting plant performance. Our findings emphasize a key role of rhizobacterial siderophores and biofilms in Fe uptake and offer mechanistic insights for microbial biofortification strategies against Fe deficiency in crops.

INTRODUCTION

One of the greatest challenges in modern agriculture is sustainably feeding the rapidly increasing population with limited land resources. Approximately 30% of the global cultivated lands consist of calcareous soils characterized by high pH and elevated bicarbonate content.[1] In these soils, crops frequently exhibit leaf chlorosis and reductions in yield and quality due to poor iron (Fe) bioavailability.[2] Moreover, Fe deficiency in crops negatively affects dietary Fe intake, leading to anemia, fatigue, poor pregnancy outcomes, and impaired cognitive development in children.[3] Consequently, Fe deficiency is among the most prevalent micronutrient deficiencies, impacting more than 2 billion people worldwide.[4]

To address potential Fe deficiency in food, strategies such as food supplementation, agronomic practices, conventional breeding, and transgenic approaches have been employed to alleviate malnutrition.[5] However, each of these methods has limitations, including high costs, environmental pollution, time-intensive implementation, and low public acceptance.[6,7] Increasing evidences suggest that microbial biofortification offers a cost-effective, environmentally sustainable strategy to enhance Fe availability in plants.[8–10]

Plants have evolved two distinct strategies for Fe uptake to adapt to Fe-limited environments. Non-graminaceous monocots and dicots, such as *Arabidopsis thaliana* and cucumber, employ a reduction-based strategy (i.e., strategy I), which involves rhizosphere acidification by H^+-ATPase 2 (AHA2), the reduction of Fe^{3+} to Fe^{2+} by FERRIC REDUCTION OXIDASE 2 (FRO2), and the root uptake of Fe^{2+} by IRON-REGULATED TRANSPORTER 1 (IRT1).[11] Additionally, graminaceous monocots, such as rice and maize, utilize a chelation-based strategy (i.e., strategy II), which involves the secretion of phytosiderophores (PSS) by TRANSPORTER OF MUGINEIC ACID 1 (TOM1) and the root uptake of the Fe^{3+}-PS complex by YELLOW STRIPE 1 (YS1) or YS1-Like (YSL).[12] The positive effects of microorganisms on plant Fe uptake were first demonstrated by comparing the Fe content in maize and sunflower grown in sterile vs. non-sterile soils.[13] Since then, numerous plant growth-promoting rhizobacteria (PGPR) have been reported to mitigate Fe deficiency stress in plants through various mechanisms. These include enhancing Fe bioavailability,[14–16] activating Fe acquisition and translocation pathways in plants,[17–19] promoting root development,[20,21] and increasing antioxidant enzymatic activities.[22,23] In general, multiple mechanisms concurrently operate to alleviate plant Fe deficiency.[17,23,24] Despite the significant role of PGPR in enhancing

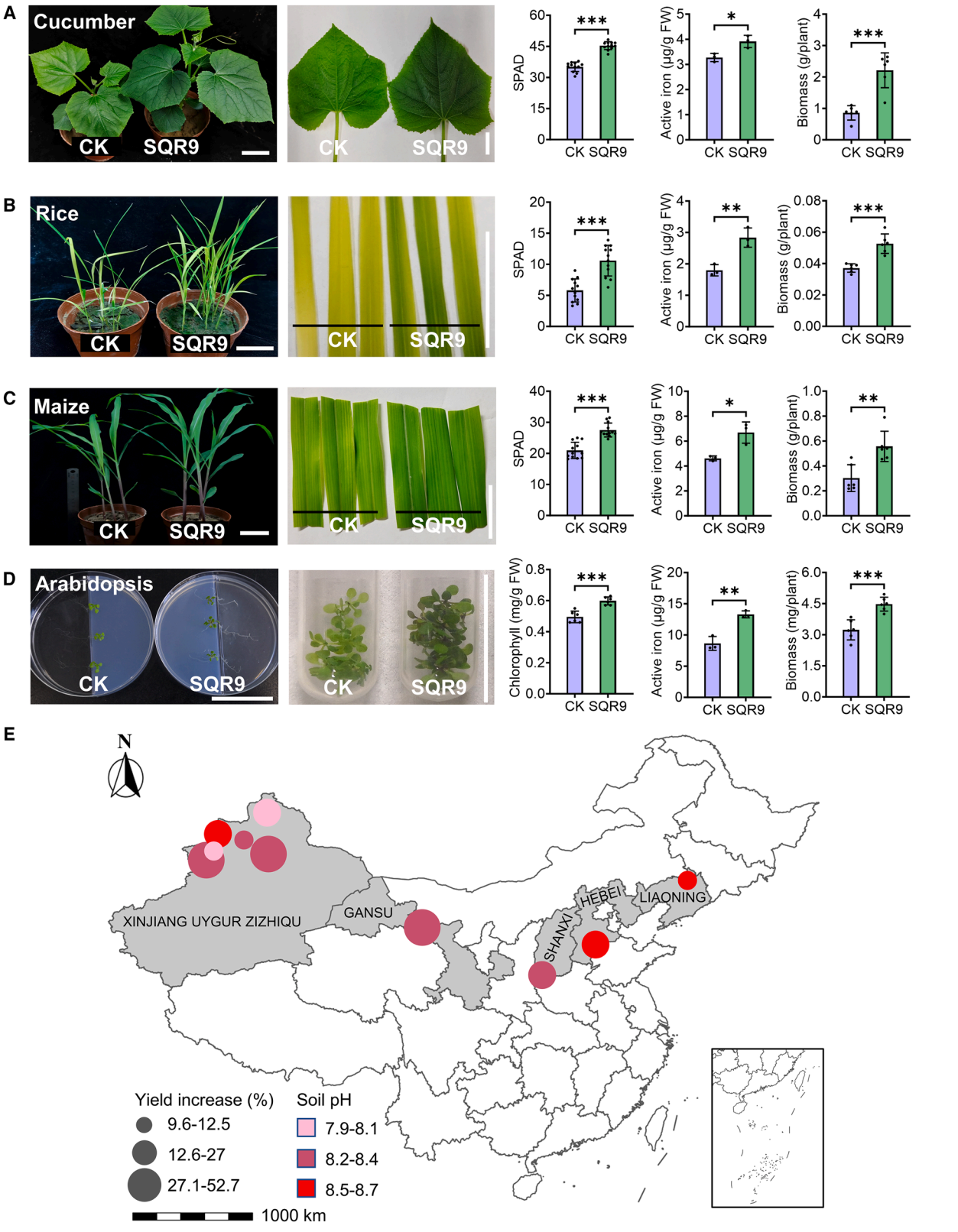

(legend on next page)

plant Fe uptake and homeostasis, the molecular mechanisms underlying these processes remain largely unknown.

Bacillus spp., widely recognized as PGPR in sustainable agriculture, confer tolerance to biotic and abiotic stress in plants.[25–27] *Bacillus velezensis* SQR9 (hereafter referred to as SQR9) is a beneficial rhizobacterium that colonizes plant roots and supports plant health by controlling diseases,[28] promoting growth,[29] and enhancing salt tolerance.[30] Similarly, *Bacillus subtilis* NCIB 3610 (hereafter referred to as 3610) promotes plant growth and antifungal resistance in melon through efficient root colonization.[31] The ability of *Bacillus* spp. to form biofilms on roots is critical for their efficient rhizosphere colonization and beneficial effects on plants.[32] Interestingly, 3610 biofilms can accumulate Fe from the environment by secreting siderophores, leading to a 10-fold higher concentration of matrix-bound Fe to intracellular Fe.[33,34] However, whether *Bacillus* biofilms accumulate Fe on roots *in situ* and whether this accumulation enhances plant Fe uptake remain unclear.

To cope with Fe shortages, bacteria secrete siderophores—small molecules with a strong affinity for ferric ions. Siderophores solubilize Fe by forming siderophore-Fe complexes, thereby increasing Fe bioavailability in the surrounding environment.[35] They are essential for PGPR in biofilm formation and root colonization.[36] In addition, siderophores produced by PGPR have long been shown to enhance plant Fe nutrition, conferring growth advantage.[37,38] For instance, pyoverdine, a siderophore from *Pseudomonas fluorescens*, significantly increases Fe concentrations in both monocotyledonous graminaceous and dicotyledonous plants, with greater efficacy than Fe-EDTA.[39,40] This raises the question of whether siderophore production during *Bacillus* biofilm formation on roots similarly benefits plant Fe acquisition.

Herein, we hypothesized that biofilm-forming *Bacillus* spp. promote plant Fe uptake through biofilm formation. We examined the emerging role of *Bacillus* biofilms in enhancing plant Fe acquisition using the biofilm-forming rhizobacterium *B. velezensis* SQR9. First, we investigated the effects of SQR9 on Fe uptake in various plants. Next, we analyzed the relationship between *Bacillus* biofilm formation and plant Fe uptake using SQR9 mutants. Finally, we elucidated the molecular mechanisms underlying the contribution of *Bacillus* biofilms to plant Fe acquisition. Our findings provide a theoretical foundation for improving crop Fe nutrition and yields in alkaline soils through biofortification strategies leveraging PGPR with strong biofilm-forming and siderophore-producing capabilities.

RESULTS

B. velezensis SQR9 promotes Fe uptake in different crops grown in calcareous soils and improves crop yields in alkaline soils across China

Plants grown in calcareous soils often exhibit chlorosis, which hinders their growth.[2] To evaluate the influence of SQR9 inoculation on crops grown in calcareous soils, cucumber, rice, and maize were tested due to their differing Fe acquisition strategies.[11,24] Remarkably, SQR9 inoculation significantly alleviated Fe deficiency-induced chlorosis in all three crops (Figures 1A–1C). In particular, compared with the control, SQR9-treated plants exhibited significant enhancement in soil and plant analyzer development (SPAD) values (29.0%–82.9%), active Fe content in young leaves (19.5%–58.0%), and dry weight (41.7%–157.9%; Figures 1A–1C).

A. thaliana, widely used for studying plant-microbe interactions,[41,42] was utilized to explore SQR9-mediated Fe uptake by the plant under controlled conditions. In both Hoagland solution and Hoagland agar in the presence of 50 μM Fe(III)EDTA, SQR9 inoculation significantly increased chlorophyll content (approximately 20.9%), active Fe content in leaves (51.3%–54.0%), and fresh weight of plants (38.4%–59.6%) compared with the uninoculated control (Figures 1D and S1). However, the chlorophyll-enhancing effect was undetectable when Fe concentration was below 50 μM (Figure S1A). Using micro X-ray fluorescence spectrometer (μ-XRF)—a non-destructive method for elemental analyses and spatial distribution,[43] we found significant differences in the spatial distribution of Fe in leaves (Figure S1E); moreover, SQR9-inoculated plants exhibited approximately 2-fold higher Fe intensity in young leaves compared with the uninoculated control (Figure S1F). These findings, corroborated by increased chlorophyll and active Fe content (Figures S1A and S1D), suggest that SQR9 inoculation enhances Fe absorption, mitigating Fe deficiency-induced chlorosis.

Crop yields are severely hampered in alkaline or calcareous soils due to Fe deficiency.[44] To evaluate the field efficacy of the SQR9 inoculation, strategy I plants, including tomato, cotton, sunflower, baby cabbage, and pepper, and strategy II plants, including wheat and maize, were cultivated in alkaline soils across five provinces in northern China (Table S1). Crops treated with SQR9 exhibited significant yield increases (9.6%–52.7%) compared with controls (Figure 1E; Table S2). Notably, SQR9 inoculation showed the most significant yield-enhancing effect on wheat in Changji, resulting in an increase of 52.7%. In contrast, the effect was weakest on cotton in Karamay and maize in Tieling, where the yield increase was approximately

Figure 1. Inoculation with *B. velezensis* SQR9 significantly mitigates the chlorotic phenotypes observed in various crops grown in calcareous soils and improves crop yields in alkaline soils across China

(A–C) Phenotypes, young leaves, SPAD values ($n = 12$), active Fe content in young leaves ($n = 3$), and dry weight ($n = 6$) of cucumber plants (A), rice plants (B), and maize plants (C) treated with or without *B. velezensis* SQR9 in calcareous soils. Scale bars, 5 cm in the phenotypes. Scale bars, 2 cm in the leaves.

(D) Phenotypes, leaves, chlorophyll content ($n = 6$), active Fe content in the leaves ($n = 3$), and fresh weight ($n = 6$) of Arabidopsis plants treated with or without SQR9 in Hoagland solution. Scale bar, 5 cm in the phenotypes. Scale bar, 2 cm in the leaves.

(E) Positive effects of SQR9 on different crop yields at 10 field sites located in the 5 provinces of northern China. The base map is from the Resource and Environment Science and Data Center, China (https://www.resdc.cn/Default.aspx), and the map approval number is GS Jing (2022) 1061. Scale bar, 1000 km. See also Tables S1 and S2.

Data are presented as mean ± SD. Significant differences were determined by Student's *t* test. $^{*}p < 0.05$, $^{**}p < 0.01$, and $^{***}p < 0.001$.

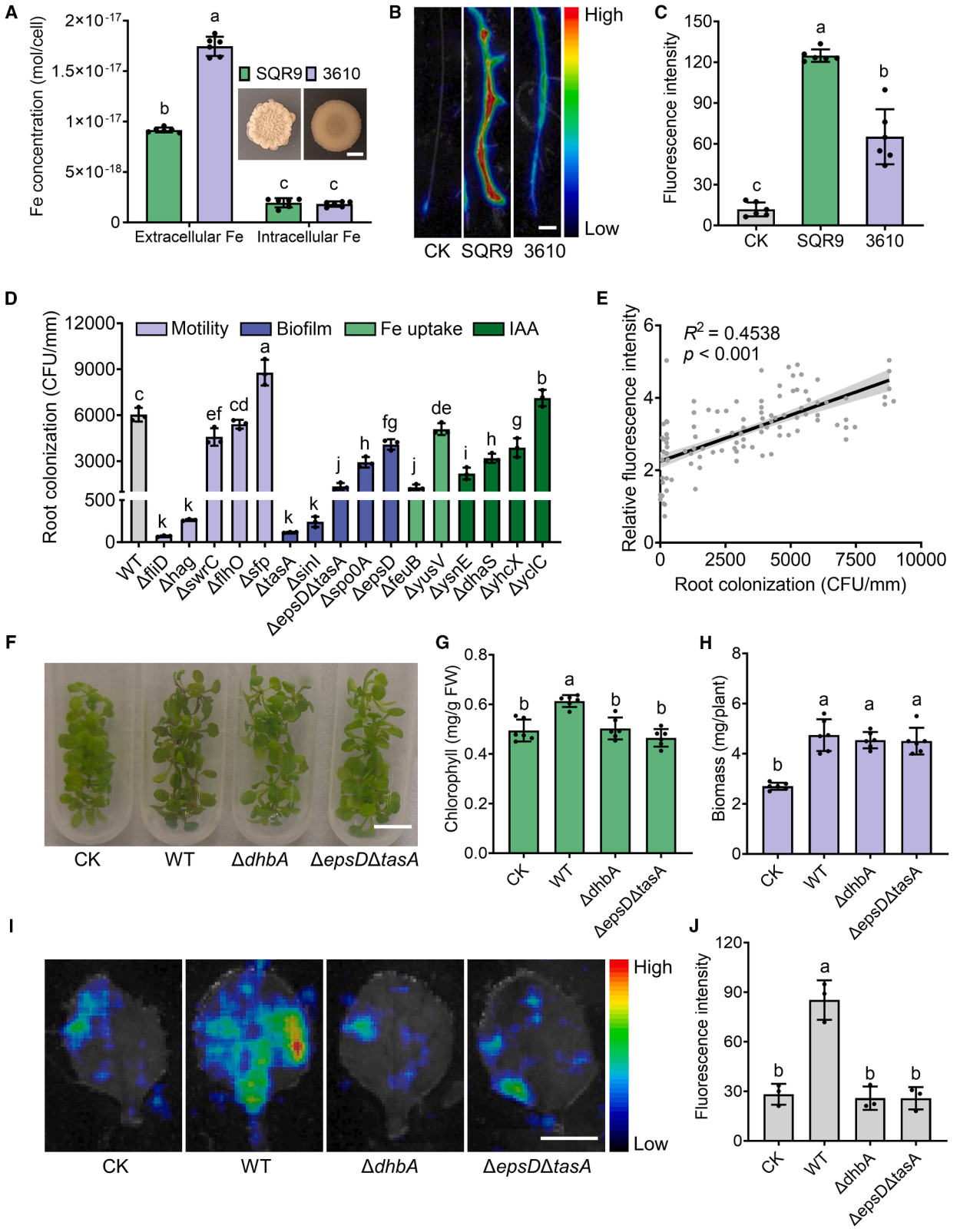

(legend on next page)

10%. Additionally, tomatoes treated with SQR9 in Tacheng exhibited a yield increase of 26.3%, while the increase in Bozhou was only 12.5%. Similarly, the yield-enhancing effects of SQR9 inoculation on wheat varied considerably across different locations, with yield increases of 52.7% in Changji, 36.7% in Yili, and 23.6% in Yuncheng (Table S2). Altogether, these findings underscore the potential of SQR9 application for enhancing crop yields in alkaline soils.

Biofilm formation by *Bacillus* contributes to enhanced plant Fe uptake

As biofilms of *B. subtilis* accumulate Fe via its siderophore,[33,34] we tested the role of SQR9 biofilms in promoting plant Fe uptake. Fe concentration within SQR9 colony biofilm was measured using inductively coupled plasma mass spectrometry (ICP-MS), with *B. subtilis* 3610 serving as a positive control. As anticipated, the biofilm-bound Fe concentrations of SQR9 and 3610 were 4.7- and 9.6-fold higher, respectively, than their intracellular Fe concentrations (Figure 2A). To confirm whether *Bacillus* biofilms accumulate Fe on roots *in situ*, biofilm-bound Fe content was quantified on Arabidopsis roots after 7 days of colonization. SQR9-treated roots exhibited higher biofilm-bound Fe levels than 3610-treated roots (Figure S2A). Besides, μ-XRF mapping revealed increased Fe intensity on SQR9-colonized roots (Figures 2B and 2C), consistent with the superior colonization ability of SQR9 under the experimental conditions (Figure S2B).

To assess the correlation between SQR9 root colonization and Fe uptake, we evaluated 16 SQR9 mutants with varying plant colonization abilities (Figure 2D; Table S3). These mutants, deficient in biofilm formation (Δ*tasA*, Δ*epsD*, Δ*epsD*Δ*tasA*, Δ*sinI*, and Δ*spo0A*),[45] Fe uptake (Δ*feuB* and Δ*yusV*),[45] motility (Δ*fliD*, Δ*hag*, Δ*swrC*, Δ*flhO*, and Δ*sfp*),[46] and indole-3-acetic acid (IAA) biosynthesis (Δ*ysnE*, Δ*dhaS*, Δ*yhcX*, and Δ*yclC*),[47] exhibited a positive correlation between SQR9 root colonization and Fe uptake under the experimental conditions (Figure 2E). Both motility and IAA production by PGPR play a vital role in efficient plant root colonization.[48,49]

Further analyses indicated that Δ*epsD*Δ*tasA* mutant, deficient in biofilm matrix production and root colonization (Figures S3A and S3E), failed to enhance chlorophyll and Fe contents in plant leaves and roots (Figures 2F, 2G, 2I, 2J, S3C and S3D) but still significantly promoted plant growth (Figure 2H). Moreover, the biofilm-bound Fe concentration in Δ*epsD*Δ*tasA* mutant was lower than that of SQR9 (Figure S3B). These results suggest that biofilm-bound Fe accumulation may be critical to SQR9-mediated Fe uptake promotion, independently of other plant growth promoting effects.

Siderophore production and biofilm matrix formation are crucial for maintaining Fe homeostasis within *Bacillus* biofilms.[50] We also evaluated the impact of Δ*dhbA* mutant, defective in the production of siderophore bacillibactin (BB), on plant Fe uptake. Δ*dhbA* mutant exhibited severe defect in biofilm formation and root colonization, similar to Δ*epsD*Δ*tasA* mutant (Figures S3A and S3E). Moreover, the biofilm-bound Fe concentration in Δ*dhbA* mutant was lower than that of SQR9 (Figure S3B). This mutant also failed to enhance plant Fe uptake to the same extent as observed for SQR9 (Figures 2F, 2G, 2I, 2J, S3C and S3D). Notably, biofilm matrix plays an important role in Fe uptake by enhancing the efficiency of siderophore utilization.[50] These results suggest that the ability of SQR9 to promote plant Fe uptake is linked, in part, to its siderophore production.

Biofilm-bound Fe is essential for SQR9 to promote plant Fe uptake

To determine the specific role of biofilm-bound Fe in promoting plant Fe uptake, we constructed Δ*abrB*Δ*dhbA* and Δ*sinR*Δ*dhbA* double mutants by allelic exchange as previously described.[46] Δ*dhbA* mutant exhibited poor biofilm formation and compromised Fe accumulation within biofilms (Figures S3A and S3B). AbrB and SinR are key repressors of biofilm formation in *Bacilli*.[51] Accordingly, Δ*abrB*Δ*dhbA* and Δ*sinR*Δ*dhbA* showed no significant defects in biofilm biomass (Figures 3A and 3B), despite reduced Fe accumulation within biofilms due to defective catecholate siderophore BB production (Figures 3C and 3D). Interestingly, Δ*abrB*Δ*dhbA* exhibited severe colonization defect, whereas Δ*sinR*Δ*dhbA* remained a strong plant root colonizer (Figure 3E). Therefore, we evaluated the effect of Δ*sinR*Δ*dhbA* on plant Fe uptake. As anticipated, Δ*sinR*Δ*dhbA* failed to

Figure 2. A positive correlation can be observed between the ability of *B. velezensis* SQR9 to form biofilms on plant roots and its efficacy in enhancing plant Fe uptake

(A) Measurement of extracellular (biofilm-bound) and intracellular Fe concentrations for cells collected from colony biofilms of *B. velezensis* SQR9 and *B. subtilis* 3610 on MSgg medium at 30°C for 48 h. Scale bar, 5 mm ($n = 6$).

(B) X-ray fluorescence mapping of Fe in Arabidopsis roots after 7 days of colonization by SQR9 and 3610. The color scale on the right shows the relative abundance of Fe. Scale bar, 1 mm.

(C) Quantification of fluorescence intensities in (B) by ImageJ ($n = 6$).

(D) Colonization of SQR9 and its derived mutants defective in motility, biofilm formation, Fe uptake, and IAA biosynthesis on Arabidopsis roots at 7 days post-inoculation ($n = 3$).

(E) Correlation between the root colonization of SQR9 and the Fe content of Arabidopsis roots ($F_{1,\ 106} = 81.64$, $p < 0.001$, $R^2 = 0.4538$). Fe content of Arabidopsis roots was indicated as the X-ray fluorescence intensity of Fe, which was normalized relative to that of the untreated control. The black line and the shaded area depict the best-fit trendline and the 95% confidence interval of the linear regression, respectively.

(F) Phenotypes of 7-day-old Arabidopsis seedlings grown with SQR9, Δ*dhbA*, and Δ*epsD*Δ*tasA* for 7 days. Scale bar, 5 mm.

(G) Chlorophyll content ($n = 6$).

(H) Plant fresh weight ($n = 6$).

(I) X-ray fluorescence mapping of Fe in young leaves. The color scale on the right shows the relative abundance of Fe. Scale bar, 1 mm.

(J) Quantification of fluorescence intensities in (I) by ImageJ ($n = 3$).

Data are presented as mean ± SD. Different letters above the column indicate significant differences according to one-way ANOVA with Duncan's multiple range test ($p < 0.05$).

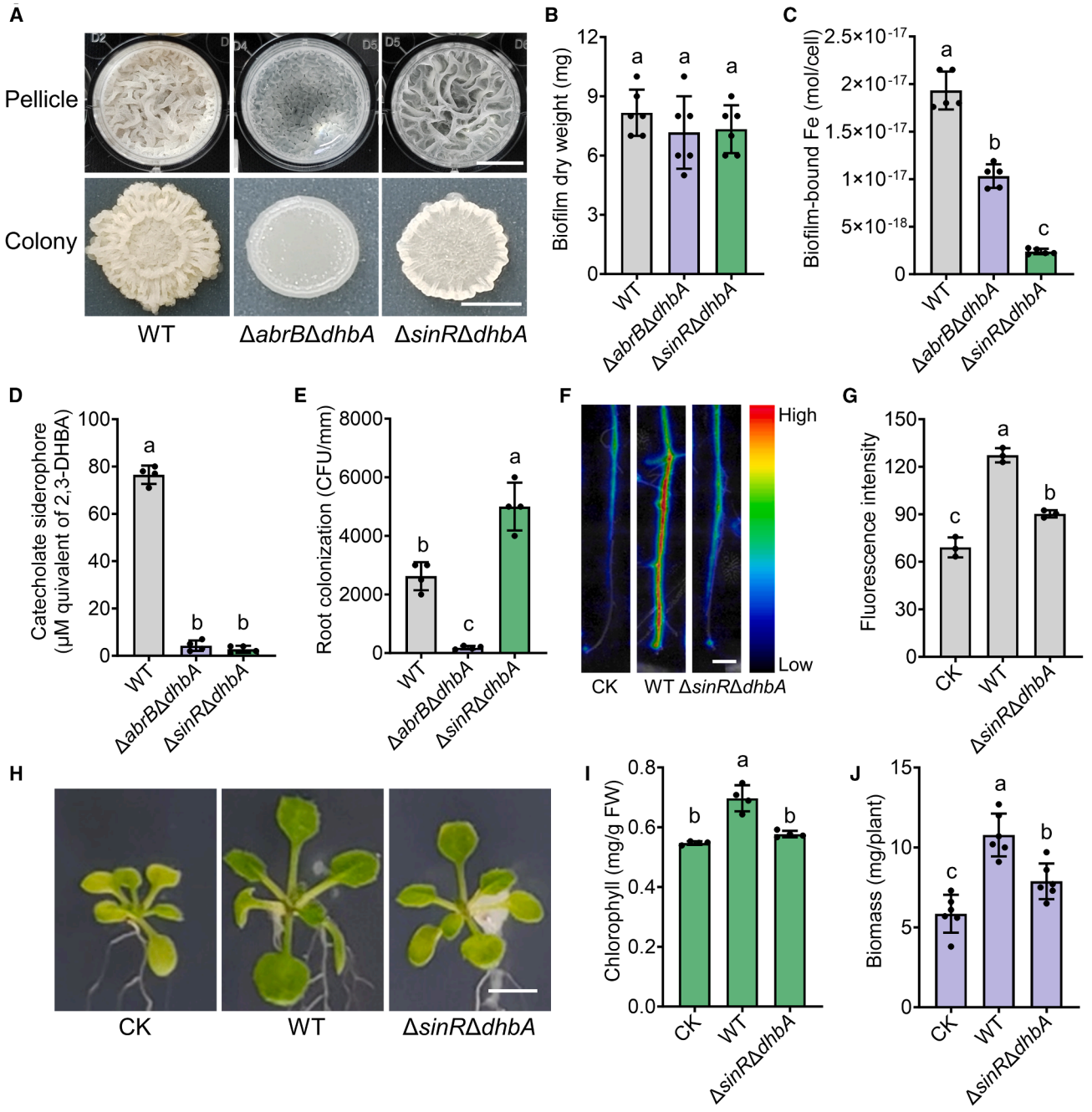

Figure 3. The siderophore bacillibactin within the biofilm, rather than the biofilm matrix or the colonization density of *Bacillus* cells, is critical for enhancing plant Fe uptake

(A) Pellicle biofilm and colony biofilm of SQR9 and its derived mutants in/on MSgg at 37°C for 48 h. Scale bars, 5 mm.

(B) Quantification of pellicle biofilms by dry weight (n = 6).

(C) Measurement of biofilm-bound Fe concentrations for cells collected from colony biofilms (n = 5).

(D) Production of the catecholate siderophore of SQR9 and its derived mutants in MKB medium at 37°C for 48 h (n = 4).

(E) Colonization of SQR9 and its derived mutants on Arabidopsis roots at 7 days post-inoculation (n = 4).

(F) X-ray fluorescence mapping of Fe in Arabidopsis roots after 7 days of colonization by SQR9 and Δ*sinR*Δ*dhbA*. The color scale on the right shows the relative abundance of Fe. Scale bar, 1 mm.

(G) Quantification of fluorescence intensities in (F) by ImageJ (n = 3).

(H) Phenotypes of Arabidopsis seedlings grown with *B. velezensis* SQR9 and Δ*sinR*Δ*dhbA*. Scale bar, 5 mm.

(legend continued on next page)

accumulate Fe on roots *in situ* (Figures 3F and 3G) and did not enhance plant greenness (Figures 3H and 3I), but it still promoted plant growth (Figure 3J). These findings were comparable to those observed for Δ*epsD*Δ*tasA* and Δ*dhbA* mutants (Figures 2F–2H, S3C and S3D), indicating that biofilm-bound Fe, rather than biofilm matrices or bacterial colonization density, is critical for enhancing plant Fe uptake.

Plants absorb Fe from the root-associated biofilm of SQR9

We further assessed whether SQR9 biofilm on roots serves as an Fe reservoir, making Fe more readily accessible to host plants. To test this hypothesis, we conducted three experiments using the stable isotope ^{57}Fe (Figures 4A–4C). First, biofilms enriched in ^{57}Fe were transferred to Arabidopsis roots (Figure 4A). After 2 days, ^{57}Fe content in Arabidopsis seedlings increased by 27.4% compared with the control, indicating that plants can absorb Fe from biofilms (Figure 4D). Next, biofilm-bound ^{57}Fe was extracted by sonication and centrifugation (Figure 4B). One chamber of the bipartite plate contained water agar to provide physical support for Arabidopsis shoots, and the other contained Hoagland solution with biofilm-bound ^{57}Fe to facilitate nutrient uptake by Arabidopsis roots. After 2 days of ^{57}Fe exposure, ^{57}Fe content in Arabidopsis seedlings increased by 17.0% compared with the control, indicative of Fe absorption from the biofilm matrix (Figure 4E). Finally, Arabidopsis seedlings were colonized by SQR9, Δ*epsD*Δ*tasA*, and Δ*sinR*Δ*dhbA* mutants for 7 days in Hoagland solution containing ^{57}Fe and then transferred to Fe-free Hoagland solution (Figure 4C). After 2 days, the shoot ^{57}Fe-increasing rates for seedlings colonized by SQR9, Δ*epsD*Δ*tasA*, and Δ*sinR*Δ*dhbA* mutants were 4.7-, 0.6-, and 2.3-fold higher than in the control, respectively (Figure 4F). Altogether, these findings indicate that plants utilize biofilms as an Fe reservoir to absorb Fe when SQR9 colonizes their roots.

SQR9 colonization activates Fe acquisition-related genes in Arabidopsis roots through siderophore production

To explore the mechanism through which SQR9 colonization enhances plant Fe acquisition, we performed RNA-seq to analyze gene expression in Arabidopsis roots colonized by SQR9 (Figure S4A). Compared with the control, the expression of 2,737 and 2,857 genes was upregulated and downregulated, respectively (false discovery rate < 0.05, fold change > 2; Figure S4B). Gene Ontology (GO) enrichment analyses in the molecular function category revealed that several differentially expressed genes (DEGs) were associated with heme binding, ion binding, catalytic activity, oxidoreductase activity, and Fe ion binding (Figure S4C), suggesting molecular-level modulation of plant Fe acquisition by SQR9 colonization. Specifically, we concentrated on the expression levels of DEGs involved in Fe homeostasis (Figure S4D). The expression of key genes related to Fe uptake, translocation, and regulation in roots was significantly upregulated by SQR9 colonization. In particular, the expression of *IRT1* and *FRO2* was upregulated by 45.3- and 16.2-fold, respectively, compared with the control (Figure S4D). Reverse transcription-quantitative PCR (RT-qPCR) approach confirmed these expression patterns, with the expression of *IRT1* and *FRO2* being upregulated by 64.4- and 10.2-fold, respectively, compared with the control (Figures 5A and S5). Moreover, the expression of coumarin biosynthesis genes (*F6′H1*, *COSY*, *S8H*, and *CYP82C4*) was upregulated by over 2-fold (Figure S5).

Furthermore, we analyzed *IRT1* expression in the roots of seedlings expressing *IRT1::H2B-2xmCherry*. SQR9 colonization significantly enhanced *IRT1::H2B-2xmCherry* expression compared with the control, with a 2.8-fold increase in fluorescence intensity (Figures S6A and S6B). To further characterize the physiological responses of plants to SQR9 colonization, we measured ferric-chelate reductase (FCR) activity and fluorescent phenolic compound production. The FCR activity of SQR9-colonized roots was 4.1-fold higher than that of the control (Figure S6C). In addition, fluorescent phenolic compound production was significantly increased by 17.8-fold compared with the control (Figures S6D and S6E). These results aligned with the observed upregulation of the expression of *IRT1*, *FRO2*, and coumarin biosynthesis genes (Figure 5A). Altogether, these results suggest that SQR9 colonization activates Fe acquisition in plants by regulating strategy I Fe-deficiency responses.

Siderophores can dissolve insoluble Fe and also trigger Fe-deficiency responses in plants.[44,52,53] The catecholate siderophore BB is critical for SQR9 to maintain Fe homeostasis and is continuously produced during biofilm formation.[45] We hypothesized that BB triggers Fe-deficiency responses in plants when SQR9 colonizes roots through biofilm formation. To test this hypothesis, we compared *IRT1* and *FRO2* expression levels in SQR9-, Δ*dhbA*-, Δ*sinR*Δ*dhbA*-, and Δ*epsD*Δ*tasA*-colonized roots using RT-qPCR. Activation of *IRT1* and *FRO2* expression was impaired in response to Δ*dhbA* and Δ*sinR*Δ*dhbA* colonization, while the expression of these Arabidopsis genes remained upregulated in response to Δ*epsD*Δ*tasA* and SQR9 colonization (Figures 5B and S7D). Meanwhile, we analyzed *IRT1* expression in the roots of seedlings expressing *IRT1::H2B-2xmCherry* when these GFP-labeled strains (including wild-type [WT] and mutants of SQR9) colonized the roots. Similar to SQR9-*gfp*, Δ*epsD*Δ*tasA*-*gfp* also significantly induced *IRT1::H2B-2xmCherry* expression, although its colonization ability was weaker. In contrast, Δ*sinR*Δ*dhbA*-*gfp* exhibited a comparable colonization ability to SQR9-*gfp*, but it compromised the increasing effect on *IRT1::H2B-2xmCherry* expression (Figures S7A–S7C). These findings were consistent with the RT-qPCR results (Figure 5B), indicating that BB, rather than the biofilm matrix or bacterial colonization density, induces Fe-deficiency responses in plants.

As purified BB was not available for our study, we used the catecholate siderophore enterobactin (ENT) to study its effects

(I) Chlorophyll content (n = 4).
(J) Plant fresh weight (n = 6).
Data are presented as mean ± SD. Different letters above the column indicate significant differences according to one-way ANOVA with Duncan's multiple range test (p < 0.05).

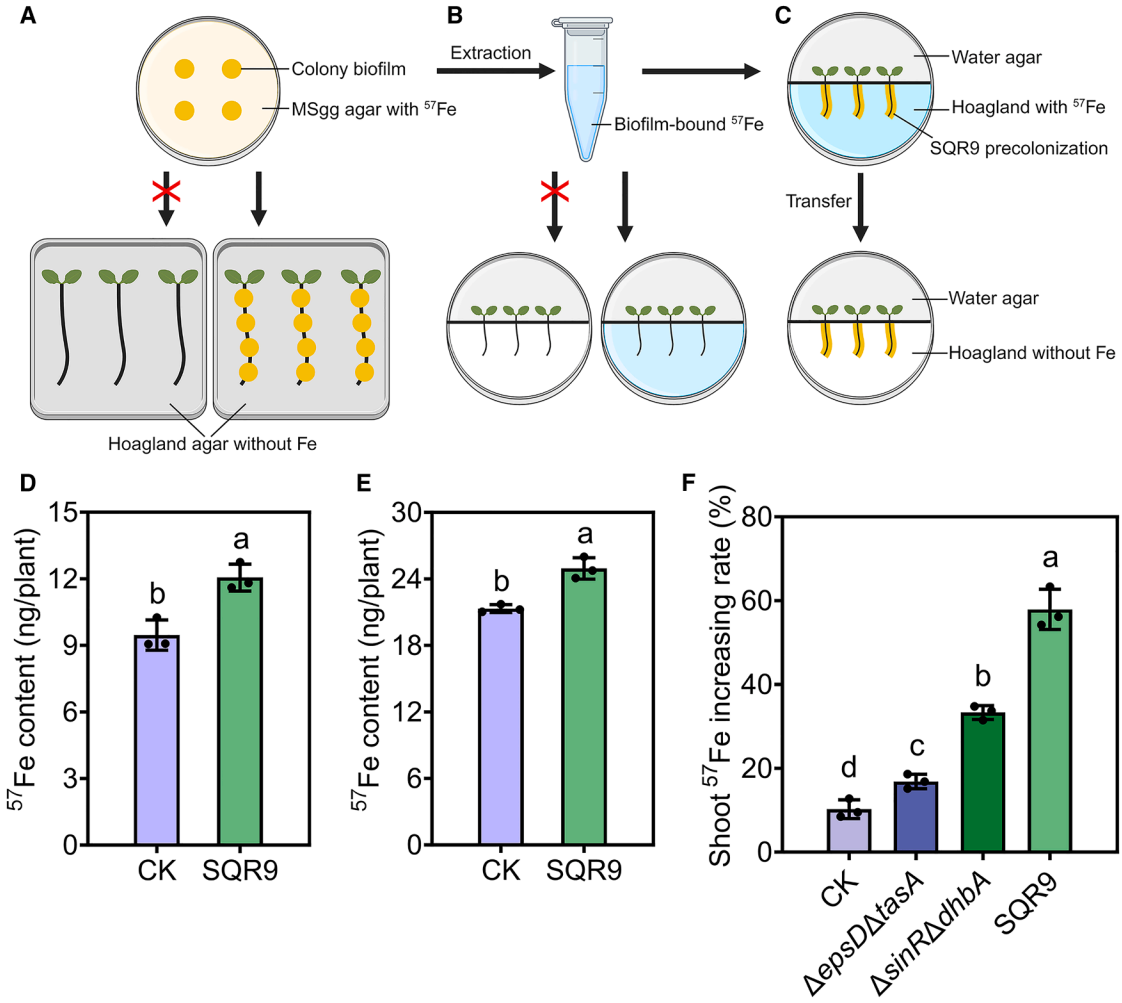

Figure 4. Fe bound within the biofilm of *B. velezensis* SQR9 can be absorbed by *A. thaliana*

(A) Schematic representation of ^{57}Fe uptake from colony biofilms to plants.

(B) Schematic representation of ^{57}Fe uptake from colony biofilm matrices to plants.

(C) Schematic representation of ^{57}Fe uptake from biofilms on roots *in situ* to plants.

(D and E) ^{57}Fe content of the whole plant in (A) and (B), respectively (n = 3).

(F) The percentage of of ^{57}Fe content increase in plant shoots after 2 days of transfer in (C) (n = 3).

Data are presented as mean ± SD. Different letters above the column indicate significant differences according to Student's t test (D and E) or one-way ANOVA with Duncan's multiple range test (F) ($p < 0.05$).

on the Fe-deficiency responses in plants. ENT and BB are structurally similar, possess comparable binding affinities for ferric Fe, and share the biosynthesis precursor 2,3-dihydroxybenzoic acid (DHBA).[54,55] DHBA, which has a lower ferric ion-binding affinity than BB, is essential for biofilm formation.[33] RT-qPCR analysis showed that treatments with DHBA and ENT both activated *IRT1* and *FRO2* expression (Figures 5C and S7E). Moreover, *IRT1* and *FRO2* expression levels under ENT treatment were significantly higher than those under DHBA treatment. Next, we analyzed *IRT1* expression in the roots of seedlings expressing *IRT1::H2B-2xmCherry*. After 1 day of treatment, *IRT1::H2B-2xmCherry* expression was significantly induced in the roots under Fe-free conditions. However, there were no notable differences between treatments with 50 μM Fe(III)EDTA and 100 μM Fe(III)EDTA (Figures 5D and 5E). Consistent with RT-qPCR results, the addition of DHBA and ENT to Hoagland solution containing 50 μM Fe(III)EDTA significantly upregulated *IRT1::H2B-2xmCherry* expression compared with the control (Figures 5C–5E). Collectively, these results suggest that catecholate siderophores play a critical role in activating plant's Fe acquisition when SQR9 colonizes roots.

SQR9 colonization enhances Fe uptake in plants via reduction-based Fe uptake system

SQR9 colonization activated Fe uptake in plants by significantly upregulating *IRT1* and *FRO2* expression. To further elucidate the importance of these genes in SQR9 colonization-mediated plant Fe uptake, we utilized Arabidopsis mutants deficient in *FRO2*

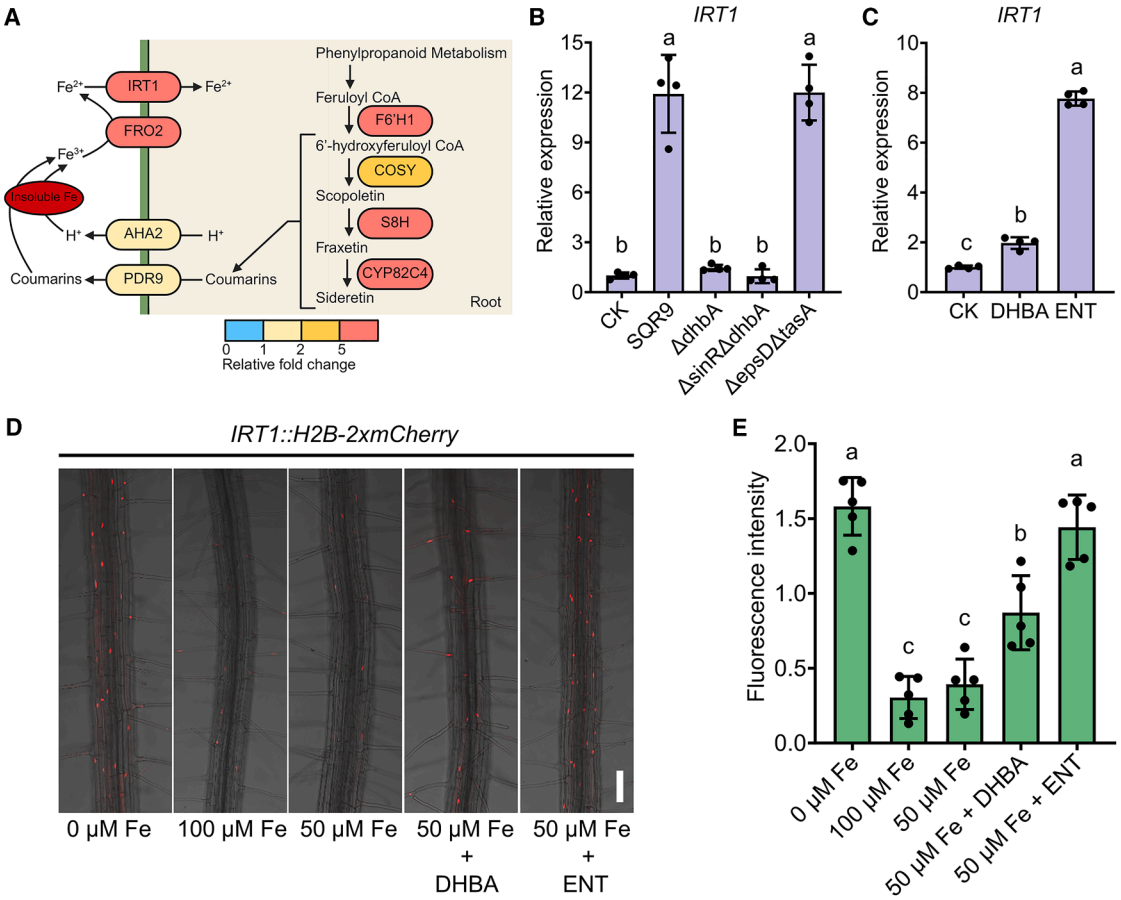

Figure 5. Catecholate siderophore, enterobactin (ENT), and the biosynthesis precursor of bacillibactin, 2,3-dihydroxybenzoic acid (DHBA) can specifically induce the expression of Fe acquisition-related genes in *A. thaliana*

(A) The relative fold change of classical Fe acquisition-related genes examined by RT-qPCR after 5 days of SQR9 colonization. The color scale represents the relative fold change of target gene expression. See also Figure S5.

(B) Relative expression of *IRT1* in Arabidopsis roots in response to the colonization of SQR9, Δ*dhbA*, Δ*sinR*Δ*dhbA*, and Δ*epsD*Δ*tasA* measured by RT-qPCR ($n = 4$).

(C) Relative expression of *IRT1* in Arabidopsis roots in response to 2,3-dihydroxybenzoic acid (DHBA) and enterobactin (ENT) measured by RT-qPCR ($n = 4$). Plant roots were collected after 24 h of treatment with or without 10 μmol/L siderophores, the concentration produced by *B. subtilis* during biofilm formation.[50]

(D) Confocal microscopy images of *IRT1::H2B-2xmCherry* in the root maturation zone of 7-day-old Arabidopsis seedlings grown with or without siderophores for 24 h. Scale bar, 100 μm.

(E) Quantification of fluorescence intensities in (D) by ImageJ ($n = 5$).

Data are presented as mean ± SD. Different letters above the column indicate significant differences according to one-way ANOVA with Duncan's multiple range test ($p < 0.05$).

(*fro2*) and *IRT1* (*irt1*), which are essential for ferric reduction and ferrous transport, respectively (Figures 5A and 6A). After 7 days of treatment, *irt1* and *fro2* mutants exhibited significantly reduced chlorophyll content compared with WT plants (Figure 6B), consistent with prior findings.[56] However, there was no difference in biomass between WT and mutant plants (Figure 6C). Unlike WT plants, SQR9 colonization failed to increase chlorophyll content in *fro2* plants (Figure 6B). In *irt1* plants, the effect of SQR9 colonization on chlorophyll content was attenuated (Figure 6B), suggesting the involvement of other Fe transport mechanisms. Interestingly, no difference was observed between WT and mutant plants in terms of promoting growth by SQR9 colonization (Figure 6C), indicating that SQR9 alleviates plant Fe deficiency independently of growth promotion. Quantitative analysis of SQR9 populations on roots, performed via CFU counting, revealed no significant differences in root colonization between of WT, *irt1*, and *fro2* plants (Figure 6D). Altogether, these results indicate that SQR9 colonization-enhanced Fe uptake in plants is entirely dependent on *FRO2* and partially on *IRT1*.

DISCUSSION

Bacteria biofilms, formed by microbial adherence via self-produced extracellular matrices, exhibit emergent properties compared with planktonic cells.[51] Biofilms play a critical role in

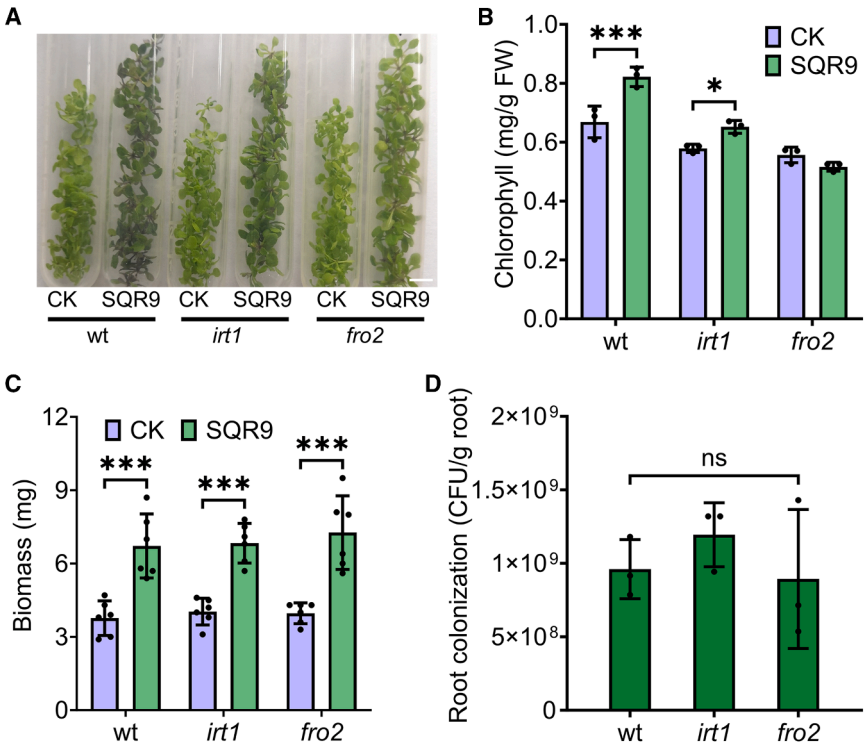

Figure 6. The Fe acquisition-related genes *IRT1* and *FRO2* in *A. thaliana* are both involved in the process by which *B. velezensis* SQR9 enhances plant Fe uptake

(A) Phenotypes of 7-day-old Arabidopsis seedlings grown with or without *B. velezensis* SQR9 for 7 days. Scale bar, 5 mm.

(B) Chlorophyll content ($n = 3$).

(C) Plant fresh weight ($n = 6$).

(D) Colonization of SQR9 on the roots of different Arabidopsis Fe uptake defective mutants at 7 days post-inoculation ($n = 3$).

Data are presented as mean ± SD. Statistical significances were determined by Student's *t* test (B and C) or one-way ANOVA with Duncan's multiple range test (D). $^{*}p < 0.05$ and $^{***}p < 0.001$. ns, not significant.

plant health, contributing to diseases inhibition,[57] drought tolerance induction,[58] and mitigation of herbicide and heavy metal toxicity.[59,60] Herein, our findings highlight the importance of *Bacillus* biofilms in promoting plant Fe uptake. We demonstrated that SQR9 biofilms contribute to plant Fe uptake by accumulating Fe. Further experimentation confirmed that this process depends on siderophore production by SQR9 and the reduction-based Fe uptake system in plants. Field experiments indicated that SQR9 significantly enhances crop yields in alkaline soils. Based on our results and previous knowledge, we propose a model illustrating how biofilm-forming SQR9 promotes plant Fe uptake in the rhizosphere (Figure 7). These findings broaden the application prospects of SQR9 as PGPR for future sustainable agriculture.

First, we observed that extracellular Fe concentrations were higher than intracellular Fe concentrations in SQR9 biofilms, similar to those in *B. subtilis* 3610 biofilms, indicating that SQR9 biofilms can accumulate Fe. This result is consistent with previous findings.[34] Extracellular Fe is essential as an electron acceptor for extracellular electron transfer in *Bacillus* biofilms.[33] Moreover, biofilm-bound Fe alleviates Fe stress in microorganisms exposed to fluctuating Fe availability in natural environments.[34] Intriguingly, SQR9 biofilms were found to accumulate Fe on roots *in situ*, suggesting that *Bacillus* biofilms on roots as an Fe reservoir, enhancing Fe accessibility for host plants. We confirmed a positive correlation between SQR9 root colonization and root Fe content using various mutants of SQR9.

Plants secrete 11%–40% of photosynthesis-derived carbon into the rhizosphere as root exudates, which recruit beneficial bacteria to colonize the roots, alleviating stress-induced adverse effects on plant growth.[36] The root surface is a highly active site for plant-microbe interactions, facilitating nutrient exchange. Previous studies have shown that SQR9 effectively colonizes the roots of various plants, including Arabidopsis,[61] cucumber,[62] maize,[63] white lupin,[64] and banana,[65] through biofilm formation. Using isotopic labeling, we demonstrated that plants absorb Fe from SQR9 biofilms colonizing their roots, suggesting that under Fe-deficient conditions, plants utilize biofilms as an Fe reservoir. Interestingly, a four-species bacterial consortium capable of synergistic biofilm production was reported to enhance drought tolerance in Arabidopsis, likely due to water retention by biofilms.[58] Biofilm formation is also crucial for biological nitrogen fixation and phosphorus solubilization in soil.[66,67] Colonization by biofilm-producing PGPR on roots leads to rhizosheath formation, helping plants to cope with water stress, and nitrogen and phosphorus deficiencies.[68] Apart from Fe, other metal ions, such as potassium, calcium, zinc, and manganese, accumulate in *Bacillus* biofilms, supporting bacterial metabolism and sporulation.[69] Future studies are required to evaluate the potential effects of these elements on plant-microbe interactions and plant growth.

Next, we found that SQR9 colonization activates Fe acquisition in plants by regulating strategy I Fe-deficiency responses. In strategy I plants, including Arabidopsis, tomato, and cucumber, Fe acquisition involves *FRO2* and *IRT1*, which reduce Fe and transport it into the roots, respectively.[2,12,24] Furthermore, our results indicated that SQR9 colonization-enhanced Fe uptake in Arabidopsis plants entirely depends on *FRO2* and partially on *IRT1*. Homology analyses have identified several *FRO2* genes in strategy II plants, such as rice, sorghum, and maize.[70] Nevertheless, the FCR activity in rice roots remains low and is not induced by Fe deficiency.[71] Although strategy II plants mainly utilize a chelation-based strategy for Fe uptake, rice, wheat, and maize also possess *IRT1* genes, which facilitate Fe uptake and translocation.[72] We demonstrated that SQR9 promotes Fe uptake in both strategy I and II plants in calcareous

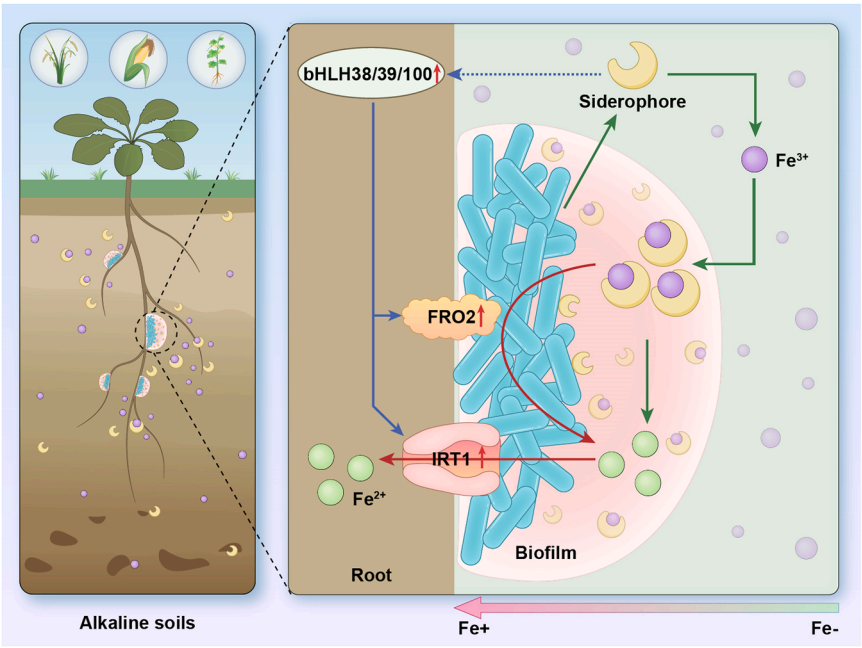

Figure 7. A model illustrating how biofilm-forming *B. velezensis* SQR9 promotes plant iron uptake in the rhizosphere

Bacillus biofilms on the roots can accumulate Fe from the environment by secreting siderophores. A large fraction of biofilm-bound Fe serves as the terminal electron acceptor in extracellular electron transfer.[33] Furthermore, plants are able to uptake Fe from the root-associated biofilm of SQR9. In addition, the siderophore bacillibactin enhances the Fe acquisition mechanisms in plants. Consequently, *Bacillus* biofilms on the roots act as an Fe reservoir, thereby increasing Fe availability to the host plant. The figure was created with BioRender.com.

soils, indicating the universality of this effect. Further investigations are required to elucidate the precise molecular mechanisms underlying SQR9-mediated Fe uptake in strategy II plants.

In addition to IRT1, NATURAL RESISTANCE-ASSOCIATED MACROPHAGE PROTEIN 1 (NRAMP1) may transport Fe^{2+} into roots,[2] while its expression was significantly downregulated in SQR9-colonized roots. Furthermore, SQR9 colonization upregulated the expression of *IRT2*, but IRT2 is not directly involved in external Fe uptake in Arabidopsis.[73] Besides the classical reduction-based strategy, Arabidopsis plants secrete Fe-mobilizing fluorescent phenolic compounds known as coumarins to improve Fe mobilization under Fe-limiting conditions.[11] A recent study has demonstrated that Fe^{3+}-coumarin complexes can be taken up by plant roots through an IRT1-independent mechanism.[74] Intriguingly, biofilm-bound Fe contains both Fe^{3+} and Fe^{2+} in nearly equal proportions. SQR9 colonization upregulated the expression of genes involved in coumarin biosynthesis (*F6′H1*, *COSY*, *S8H*, and *CYP82C4*) and secretion (*PDR9*). More fluorescent phenolic compounds were also detected in root exudates of SQR9-colonized plants. It remains possible that coumarins may facilitate Fe transport from biofilms to plants. Similarly, previous studies have demonstrated that *Bacillus* sp. WR12, *Azospirillum brasilense* DSM-1843, and *Paenibacillus polymyxa* BFKC01 can significantly enhance the release of fluorescent phenolic compounds in plants in response to Fe deficiency.[4,20,75] Further work is required to elucidate the potential role of coumarins in SQR9-mediated Fe uptake in plants.

Finally, our findings suggested that BB plays a critical role in activating plant Fe acquisition during SQR9 colonization. This activation likely results from the Fe-chelating capacity of siderophores.[52,53] Similarly, BB produced by *B. subtilis* induces Fe mobilization responses in rice through YELLOW STRIPE-LIKE 15 (YSL15), which transports the PS-Fe^{3+} complex from the rhizosphere into roots.[76] While the concentration of BB produced by *Bacillus* during biofilm formation in the MSgg medium has been quantified,[50] its levels during root colonization by SQR9 remain unexplored. The colonization of PGPR on roots via biofilm formation is markedly influenced by the abundance and composition of root exudates, which vary across different root zones.[36] Therefore, the concentration of BB is likely to exhibit spatial heterogeneity in the rhizosphere. Moreover, the production of BB by *Bacillus* is also modulated by Fe availability in the surrounding environment.[77] Siderophores have long been shown to enhance plant Fe nutrition by increasing Fe bioavailability.[37,38] Intriguingly, plants possess the ability to exude fluorescent phenolic compounds into the rhizosphere, which serve to recruit siderophore-producing microbes. This interaction subsequently promotes plant Fe acquisition through microbial siderophores.[78] In addition, a pot experiment has demonstrated that BB from *Bacillus* strains promotes Fe absorption and plant growth in sesame.[79] Meanwhile, *in silico* analyses have revealed stronger binding affinity of BB-Fe^{3+} complexes to YSL15 in rice than PS-Fe^{3+} complexes, suggesting the potential role of YSL15 in the uptake of BB-Fe^{3+} complexes.[80] Future studies should explore the potential of purified BB from *Bacillus* strains for Fe biofortification across diverse crops.

To summarize, we report that SQR9 accumulates Fe on roots through biofilm formation and activates plant Fe acquisition mechanisms through siderophore production. Fe in SQR9 biofilms can be absorbed by plants, providing mechanistic insights into the molecular details underlying biofilm-forming PGPR-mediated Fe uptake. Our findings also highlight the potential of PGPR with robust biofilm-forming and siderophore-producing abilities for Fe biofortification in sustainable agriculture.

Limitations of the study

Our results have shown that *B. velezensis* SQR9 biofilms accumulate Fe on plant roots through the siderophore BB, thereby enhancing plant Fe nutrition. While BB simultaneously stimulates plant Fe acquisition mechanisms, this process is partially dependent on *IRT1*. Therefore, further research is required to elucidate other mechanisms of Fe transport from biofilms to plants, such as coumarin-mediated Fe uptake. Additionally, we investigated

the effect of BB on plant Fe acquisition using the siderophore ENT as a substitute. Further studies are needed to determine how BB stimulates plant Fe acquisition mechanisms and whether BB-Fe^{3+} complexes can be directly absorbed and utilized by plants.

RESOURCE AVAILABILITY

Lead contact

Requests for further information and resources should be directed to and will be fulfilled by the lead contact, Qirong Shen (shenqirong@njau.edu.cn).

Materials availability

All unique/stable reagents generated in this study are available from the lead contact without restriction.

Data and code availability

- The genome sequence of *B. velezensis* SQR9 has been deposited at the NCBI under accession number CP006890. Raw data for the plant RNA-seq have been deposited at the NCBI Sequence Read Archive (SRA) under accession number PRJNA1083752. They are publicly available as of the date of publication. The accession numbers are also listed in the key resources table.
- This paper does not report original code.
- Any additional information required to reanalyze the data reported in this paper is available from the lead contact upon request.

ACKNOWLEDGMENTS

This work was financially supported by the National Natural Science Foundation of China (42477310) and the National Key Research and Development Program of China (2022YFF1001800 and 2022YFD1500202).

AUTHOR CONTRIBUTIONS

T.T., Z.X., R.Z., and Q.S. conceptualized the project. Z.X., R.Z., and Q.S. supervised the research. T.T., L.T., X.S., and J.X. performed the experiments. Y.M., N.Z., W.X., Y.Y., Y.L., and W.R. validated the data. T.T. and Z.X. wrote the original draft of the manuscript. P.B.B. and A.T.K. reviewed and edited the manuscript. T.T. and Z.X. contributed equally to this work.

DECLARATION OF INTERESTS

The authors declare no competing interests.

STAR★METHODS

Detailed methods are provided in the online version of this paper and include the following:

SUPPLEMENTAL INFORMATION

Supplemental information can be found online at https://doi.org/10.1016/j.celrep.2025.116481.

Received: April 30, 2025
Revised: September 24, 2025
Accepted: October 3, 2025

REFERENCES

1. Zuo, Y., and Zhang, F. (2011). Soil and crop management strategies to prevent iron deficiency in crops. Plant Soil *339*, 83–95. https://doi.org/10.1007/s11104-010-0566-0.
2. Zhang, X., Zhang, D., Sun, W., and Wang, T. (2019). The adaptive mechanism of plants to iron deficiency via iron uptake, transport, and homeostasis. Int. J. Mol. Sci. *20*, 2424. https://doi.org/10.3390/ijms20102424.
3. Sahu, S.K. (2024). Maize gets an iron boost: Biofortification breakthrough holds promise to combat iron deficiency. J. Integr. Plant Biol. *66*, 635–637. https://doi.org/10.1111/jipb.13623.
4. Yue, Z., Chen, Y., Hao, Y., Wang, C., Zhang, Z., Chen, C., Liu, H., Liu, Y., Li, L., and Sun, Z. (2022). *Bacillus* sp. WR12 alleviates iron deficiency in wheat via enhancing siderophore- and phenol-mediated iron acquisition in roots. Plant Soil *471*, 247–260. https://doi.org/10.1007/s11104-021-05218-y.
5. Ofori, K.F., Antoniello, S., English, M.M., and Aryee, A.N.A. (2022). Improving nutrition through biofortification–A systematic review. Front. Nutr. *9*, 1043655. https://doi.org/10.3389/fnut.2022.1043655.
6. Murgia, I., Arosio, P., Tarantino, D., and Soave, C. (2012). Biofortification for combating "hidden hunger" for iron. Trends Plant Sci. *17*, 47–55. https://doi.org/10.1016/j.tplants.2011.10.003.
7. Avnee, S.,S., Sood, S., Chaudhary, D.R., Jhorar, P., and Rana, R.S. (2023). Biofortification : an approach to eradicate micronutrient deficiency. Front. Nutr. *10*, 1233070. https://doi.org/10.3389/fnut.2023.1233070.
8. Jin, C.W., Ye, Y.Q., and Zheng, S.J. (2014). An underground tale: contribution of microbial activity to plant iron acquisition via ecological processes. Ann. Bot. *113*, 7–18. https://doi.org/10.1093/aob/mct249.
9. Singh, D., and Prasanna, R. (2020). Potential of microbes in the biofortification of Zn and Fe in dietary food grains. Agron. Sustain. Dev. *40*, 15. https://doi.org/10.1007/s13593-020-00619-2.
10. Lurthy, T., Pivato, B., Lemanceau, P., and Mazurier, S. (2021). Importance of the rhizosphere microbiota in iron biofortification of plants. Front. Plant Sci. *12*, 744445. https://doi.org/10.3389/fpls.2021.744445.
11. Liang, G. (2022). Iron uptake, signaling, and sensing in plants. Plant Commun. *3*, 100349. https://doi.org/10.1016/j.xplc.2022.100349.
12. Gao, F., and Dubos, C. (2021). Transcriptional integration of plant responses to iron availability. J. Exp. Bot. *72*, 2056–2070. https://doi.org/10.1093/jxb/eraa556.
13. Masalha, J., Kosegarten, H., Elmaci, Ö., and Mengel, K. (2000). The central role of microbial activity for iron acquisition in maize and sunflower. Biol. Fertil. Soils *30*, 433–439. https://doi.org/10.1007/s003740050021.
14. İpek, M., Aras, S., Arıkan, Ş., Eşitken, A., Pırlak, L., Dönmez, M.F., and Turan, M. (2017). Root plant growth promoting rhizobacteria inoculations increase ferric chelate reductase (FC-R) activity and Fe nutrition in pear under calcareous soil conditions. Sci. Hortic. *219*, 144–151. https://doi.org/10.1016/j.scienta.2017.02.043.
15. Ferreira, C.M.H., Sousa, C.A., Sanchis-Pérez, I., López-Rayo, S., Barros, M.T., Soares, H.M.V.M., and Lucena, J.J. (2019). Calcareous soil interactions of the iron(III) chelates of DPH and Azotochelin and its application on

amending iron chlorosis in soybean (*Glycine max*). Sci. Total Environ. *647*, 1586–1593. https://doi.org/10.1016/j.scitotenv.2018.08.069.

16. Liu, Y., Shi, A., Chen, Y., Xu, Z., Liu, Y., Yao, Y., Wang, Y., and Jia, B. (2025). Beneficial microorganisms: Regulating growth and defense for plant welfare. Plant Biotechnol. J. *23*, 986–998. https://doi.org/10.1111/pbi.14554.
17. Zhang, H., Sun, Y., Xie, X., Kim, M.S., Dowd, S.E., and Paré, P.W. (2009). A soil bacterium regulates plant acquisition of iron via deficiency-inducible mechanisms. Plant J. *58*, 568–577. https://doi.org/10.1111/j.1365-313X.2009.03803.x.
18. Singh, D., Geat, N., Rajawat, M.V.S., Mahajan, M.M., Prasanna, R., Singh, S., Kaushik, R., Singh, R.N., Kumar, K., and Saxena, A.K. (2018). Deciphering the mechanisms of endophyte-mediated biofortification of Fe and Zn in wheat. J. Plant Growth Regul. *37*, 174–182. https://doi.org/10.1007/s00344-017-9716-4.
19. Zhou, C., Zhu, L., Guo, J., Xiao, X., Ma, Z., and Wang, J. (2019). *Bacillus subtilis* STU6 ameliorates iron deficiency in tomato by enhancement of polyamine-mediated iron remobilization. J. Agric. Food Chem. *67*, 320–330. https://doi.org/10.1021/acs.jafc.8b05851.
20. Zhou, C., Guo, J., Zhu, L., Xiao, X., Xie, Y., Zhu, J., Ma, Z., and Wang, J. (2016). *Paenibacillus polymyxa* BFKC01 enhances plant iron absorption via improved root systems and activated iron acquisition mechanisms. Plant Physiol. Biochem. *105*, 162–173. https://doi.org/10.1016/j.plaphy.2016.04.025.
21. Sonbarse, P.P., Sharma, P., and Parvatam, G. (2017). PGPR's mix treatment to moringa improved plant growth and iron content in foliage as substantiated by biochemical and molecular methods. J. Plant Interact. *12*, 526–532. https://doi.org/10.1080/17429145.2017.1400125.
22. Zhou, C., Zhu, L., Ma, Z., and Wang, J. (2018). Improved iron acquisition of *Astragalus sinicus* under low iron-availability conditions by soil-borne bacteria *Burkholderia cepacia*. J. Plant Interact. *13*, 9–20. https://doi.org/10.1080/17429145.2017.1407000.
23. Kong, W.-L., Wang, Y.-H., Lu, L.-X., Li, P.-S., Zhang, Y., and Wu, X.-Q. (2022). *Rahnella aquatilis* JZ-GX1 alleviates iron deficiency chlorosis in *Cinnamomum camphora* by secreting desferrioxamine and reshaping the soil fungal community. Front. Plant Sci. *13*, 960750. https://doi.org/10.3389/fpls.2022.960750.
24. Pii, Y., Marastoni, L., Springeth, C., Fontanella, M.C., Beone, G.M., Cesco, S., and Mimmo, T. (2016). Modulation of Fe acquisition process by Azospirillum brasilense in cucumber plants. Environ. Exp. Bot. *130*, 216–225. https://doi.org/10.1016/j.envexpbot.2016.06.011.
25. Patani, A., Patel, M., Islam, S., Yadav, V.K., Prajapati, D., Yadav, A.N., Sahoo, D.K., and Patel, A. (2024). Recent advances in *Bacillus*-mediated plant growth enhancement: a paradigm shift in redefining crop resilience. World J. Microbiol. Biotechnol. *40*, 77. https://doi.org/10.1007/s11274-024-03903-5.
26. Zhang, N., Wang, Z., Shao, J., Xu, Z., Liu, Y., Xun, W., Miao, Y., Shen, Q., and Zhang, R. (2023). Biocontrol mechanisms of *Bacillus* : Improving the efficiency of green agriculture. Microb. Biotechnol. *16*, 2250–2263. https://doi.org/10.1111/1751-7915.14348.
27. Saxena, A.K., Kumar, M., Chakdar, H., Anuroopa, N., and Bagyaraj, D.J. (2020). *Bacillus* species in soil as a natural resource for plant health and nutrition. J. Appl. Microbiol. *128*, 1583–1594. https://doi.org/10.1111/jam.14506.
28. Xu, Z., Zhang, R., Wang, D., Qiu, M., Feng, H., Zhang, N., and Shen, Q. (2014). Enhanced control of cucumber wilt disease by Bacillus amyloliquefaciens SQR9 by altering the regulation of its DegU phosphorylation. Appl. Environ. Microbiol. *80*, 2941–2950. https://doi.org/10.1128/AEM.03943-13.
29. Liu, Y., Chen, L., Zhang, N., Li, Z., Zhang, G., Xu, Y., Shen, Q., and Zhang, R. (2016). Plant-microbe communication enhances auxin biosynthesis by a root-associated bacterium, *Bacillus amyloliquefaciens* SQR9. Mol. Plant Microbe Interact. *29*, 324–330. https://doi.org/10.1094/MPMI-10-15-0239-R.
30. Chen, L., Liu, Y., Wu, G., Zhang, N., Shen, Q., and Zhang, R. (2017). Beneficial rhizobacterium *Bacillus amyloliquefaciens* SQR9 induces plant salt tolerance through spermidine production. Mol. Plant Microbe Interact. *30*, 423–432. https://doi.org/10.1094/MPMI-02-17-0027-R.
31. Berlanga-Clavero, M.V., Molina-Santiago, C., Caraballo-Rodríguez, A.M., Petras, D., Díaz-Martínez, L., Pérez-García, A., de Vicente, A., Carrión, V. J., Dorrestein, P.C., and Romero, D. (2022). *Bacillus subtilis* biofilm matrix components target seed oil bodies to promote growth and anti-fungal resistance in melon. Nat. Microbiol. *7*, 1001–1015. https://doi.org/10.1038/s41564-022-01134-8.
32. Blake, C., Christensen, M.N., and Kovács, Á.T. (2021). Molecular aspects of plant growth promotion and protection by *Bacillus subtilis*. Mol. Plant Microbe Interact. *34*, 15–25. https://doi.org/10.1094/MPMI-08-20-0225-CR.
33. Qin, Y., He, Y., She, Q., Larese-Casanova, P., Li, P., and Chai, Y. (2019). Heterogeneity in respiratory electron transfer and adaptive iron utilization in a bacterial biofilm. Nat. Commun. *10*, 3702. https://doi.org/10.1038/s41467-019-11681-0.
34. Rizzi, A., Leroux, J., Charron-Lamoureux, V., Roy, S., Beauregard, P.B., and Bellenger, J.P. (2020). *Bacillus subtilis* modulates its usage of biofilm-bound iron in response to environmental iron availability. Appl. Environ. Microbiol. *86*, e00944-20. https://doi.org/10.1128/AEM.00944-20.
35. Kramer, J., Özkaya, Ö., and Kümmerli, R. (2020). Bacterial siderophores in community and host interactions. Nat. Rev. Microbiol. *18*, 152–163. https://doi.org/10.1038/s41579-019-0284-4.
36. Liu, Y., Xu, Z., Chen, L., Xun, W., Shu, X., Chen, Y., Sun, X., Wang, Z., Ren, Y., Shen, Q., and Zhang, R. (2024). Root colonization by beneficial rhizobacteria. FEMS Microbiol. Rev. *48*, fuad066. https://doi.org/10.1093/femsre/fuad066.
37. Sharma, A., Johri, B.N., Sharma, A.K., and Glick, B.R. (2003). Plant growth-promoting bacterium *Pseudomonas* sp. strain GRP3 influences iron acquisition in mung bean (*Vigna radiata* L. Wilzeck). Soil Biol. Biochem. *35*, 887–894. https://doi.org/10.1016/S0038-0717(03)00119-6.
38. Radzki, W., Gutierrez Mañero, F.J., Algar, E., Lucas García, J.A., García-Villaraco, A., and Ramos Solano, B. (2013). Bacterial siderophores efficiently provide iron to iron-starved tomato plants in hydroponics culture. Antonie Leeuwenhoek *104*, 321–330. https://doi.org/10.1007/s10482-013-9954-9.
39. Vansuyt, G., Robin, A., Briat, J.F., Curie, C., and Lemanceau, P. (2007). Iron acquisition from Fe-pyoverdine by *Arabidopsis thaliana*. Mol. Plant Microbe Interact. *20*, 441–447. https://doi.org/10.1094/MPMI-20-4-0441.
40. Shirley, M., Avoscan, L., Bernaud, E., Vansuyt, G., and Lemanceau, P. (2011). Comparison of iron acquisition from Fe-pyoverdine by strategy I and strategy II plants. Botany *89*, 731–735. https://doi.org/10.1139/b11-054.
41. Li, Y., Shao, J., Xie, Y., Jia, L., Fu, Y., Xu, Z., Zhang, N., Feng, H., Xun, W., Liu, Y., et al. (2021). Volatile compounds from beneficial rhizobacteria *Bacillus* spp. promote periodic lateral root development in Arabidopsis. Plant Cell Environ. *44*, 1663–1678. https://doi.org/10.1111/pce.14021.
42. Li, Y., Shao, J., Fu, Y., Chen, Y., Wang, H., Xu, Z., Feng, H., Xun, W., Liu, Y., Zhang, N., et al. (2022). The volatile cedrene from *Trichoderma guizhouense* modulates Arabidopsis root development through auxin transport and signalling. Plant Cell Environ. *45*, 969–984. https://doi.org/10.1111/pce.14230.
43. Ren, Z.-W., Yang, M., McKenna, B.A., Lian, X.-M., Zhao, F.-J., Kopittke, P. M., Lombi, E., and Wang, P. (2023). Fast X-ray fluorescence microscopy provides high-throughput phenotyping of element distribution in seeds. Plant Physiol. *191*, 1520–1534. https://doi.org/10.1093/plphys/kiac534.
44. Wang, N., Wang, T., Chen, Y., Wang, M., Lu, Q., Wang, K., Dou, Z., Chi, Z., Qiu, W., Dai, J., et al. (2024). Microbiome convergence enables siderophore-secreting-rhizobacteria to improve iron nutrition and yield of peanut intercropped with maize. Nat. Commun. *15*, 839. https://doi.org/10.1038/s41467-024-45207-0.

45. Xu, Z., Mandic-Mulec, I., Zhang, H., Liu, Y., Sun, X., Feng, H., Xun, W., Zhang, N., Shen, Q., and Zhang, R. (2019). Antibiotic bacillomycin D affects iron acquisition and biofilm formation in *Bacillus velezensis* through a Btr-mediated FeuABC-dependent pathway. Cell Rep. *29*, 1192–1202. e5. https://doi.org/10.1016/j.celrep.2019.09.061.

46. Liu, Y., Huang, R., Chen, Y., Miao, Y., Štefanič, P., Mandic-Mulec, I., Zhang, R., Shen, Q., and Xu, Z. (2022). Involvement of flagellin in kin recognition between *Bacillus velezensis* strains. mSystems *7*, e00778-22. https://doi.org/10.1128/msystems.00778-22.

47. Shao, J., Li, S., Zhang, N., Cui, X., Zhou, X., Zhang, G., Shen, Q., and Zhang, R. (2015). Analysis and cloning of the synthetic pathway of the phytohormone indole-3-acetic acid in the plant-beneficial *Bacillus amyloliquefaciens* SQR9. Microb. Cell Fact. *14*, 130. https://doi.org/10.1186/s12934-015-0323-4.

48. Huang, R., Feng, H., Xu, Z., Zhang, N., Liu, Y., Shao, J., Shen, Q., and Zhang, R. (2022). Identification of adhesins in plant beneficial rhizobacteria *Bacillus velezensis* SQR9 and their effect on root colonization. Mol. Plant Microbe Interact. *35*, 64–72. https://doi.org/10.1094/MPMI-09-21-0234-R.

49. Tzipilevich, E., Russ, D., Dangl, J.L., and Benfey, P.N. (2021). Plant immune system activation is necessary for efficient root colonization by auxin-secreting beneficial bacteria. Cell Host Microbe *29*, 1507–1520. e4. https://doi.org/10.1016/j.chom.2021.09.005.

50. Rizzi, A., Roy, S., Bellenger, J.P., and Beauregard, P.B. (2019). Iron homeostasis in *Bacillus subtilis* requires siderophore production and biofilm formation. Appl. Environ. Microbiol. *85*, e02439-18. https://doi.org/10.1128/AEM.02439-18.

51. Arnaouteli, S., Bamford, N.C., Stanley-Wall, N.R., and Kovács, Á.T. (2021). *Bacillus subtilis* biofilm formation and social interactions. Nat. Rev. Microbiol. *19*, 600–614. https://doi.org/10.1038/s41579-021-00540-9.

52. Trapet, P., Avoscan, L., Klinguer, A., Pateyron, S., Citerne, S., Chervin, C., Mazurier, S., Lemanceau, P., Wendehenne, D., and Besson-Bard, A. (2016). The *Pseudomonas fluorescens* siderophore pyoverdine weakens *Arabidopsis thaliana* defense in favor of growth in iron-deficient conditions. Plant Physiol. *171*, 675–693. https://doi.org/10.1104/pp.15.01537.

53. Aznar, A., Chen, N.W.G., Rigault, M., Riache, N., Joseph, D., Desmaële, D., Mouille, G., Boutet, S., Soubigou-Taconnat, L., Renou, J.P., et al. (2014). Scavenging iron: A novel mechanism of plant immunity activation by microbial siderophores. Plant Physiol. *164*, 2167–2183. https://doi.org/10.1104/pp.113.233585.

54. Dertz, E.A., Xu, J., Stintzi, A., and Raymond, K.N. (2006). Bacillibactin-mediated iron transport in *Bacillus subtilis*. J. Am. Chem. Soc. *128*, 22–23. https://doi.org/10.1021/ja055898c.

55. Ollinger, J., Song, K.B., Antelmann, H., Hecker, M., and Helmann, J.D. (2006). Role of the Fur regulon in iron transport in *Bacillus subtilis*. J. Bacteriol. *188*, 3664–3673. https://doi.org/10.1128/JB.188.10.3664-3673.2006.

56. Harbort, C.J., Hashimoto, M., Inoue, H., Niu, Y., Guan, R., Rombolà, A.D., Kopriva, S., Voges, M.J.E.E.E., Sattely, E.S., Garrido-Oter, R., and Schulze-Lefert, P. (2020). Root-secreted coumarins and the microbiota interact to improve iron nutrition in Arabidopsis. Cell Host Microbe *28*, 825–837.e6. https://doi.org/10.1016/j.chom.2020.09.006.

57. Fessia, A., Barra, P., Barros, G., and Nesci, A. (2022). Could *Bacillus* biofilms enhance the effectivity of biocontrol strategies in the phyllosphere? J. Appl. Microbiol. *133*, 2148–2166. https://doi.org/10.1111/jam.15596.

58. Yang, N., Nesme, J., Røder, H.L., Li, X., Zuo, Z., Petersen, M., Burmølle, M., and Sørensen, S.J. (2021). Emergent bacterial community properties induce enhanced drought tolerance in Arabidopsis. npj Biofilms Microbiomes *7*, 82. https://doi.org/10.1038/s41522-021-00253-0.

59. Xiong, Z., Zheng, J., Sun, H., Hu, J., Sheng, X., and He, L. (2022). Biofilm-overproducing *Bacillus amyloliquefaciens* P29ΔsinR decreases Pb availability and uptake in lettuce in Pb-polluted soil. J. Environ. Manage. *302*, 114016. https://doi.org/10.1016/j.jenvman.2021.114016.

60. Zhang, H., Qian, Y., Fan, D., Tian, Y., and Huang, X. (2022). Biofilm formed by *Hansschlegelia zhihuaiae* S113 on root surface mitigates the toxicity of bensulfuron-methyl residues to maize. Environ. Pollut. *292*, 118366. https://doi.org/10.1016/j.envpol.2021.118366.

61. Sun, X., Xu, Z., Xie, J., Hesselberg-Thomsen, V., Tan, T., Zheng, D., Strube, M.L., Dragoš, A., Shen, Q., Zhang, R., and Kovács, Á.T. (2022). *Bacillus velezensis* stimulates resident rhizosphere *Pseudomonas stutzeri* for plant health through metabolic interactions. ISME J. *16*, 774–787. https://doi.org/10.1038/s41396-021-01125-3.

62. Xu, Z., Zhang, H., Sun, X., Liu, Y., Yan, W., Xun, W., Shen, Q., and Zhang, R. (2019). *Bacillus velezensis* wall teichoic acids are required for biofilm formation and root colonization. Appl. Environ. Microbiol. *85*, e02116-18. https://doi.org/10.1128/AEM.02116-18.

63. Zhang, N., Yang, D., Wang, D., Miao, Y., Shao, J., Zhou, X., Xu, Z., Li, Q., Feng, H., Li, S., et al. (2015). Whole transcriptomic analysis of the plant-beneficial rhizobacterium *Bacillus amyloliquefaciens* SQR9 during enhanced biofilm formation regulated by maize root exudates. BMC Genom. *16*, 685. https://doi.org/10.1186/s12864-015-1825-5.

64. Yang, J., Li, S., Zhou, X., Du, C., Fang, J., Li, X., Zhao, J., Ding, F., Wang, Y., Zhang, Q., et al. (2025). *Bacillus amyloliquefaciens* promotes cluster root formation of white lupin under low phosphorus by mediating auxin levels. Plant Physiol. *197*, kiae676. https://doi.org/10.1093/plphys/kiae676.

65. Nan, Z., Kai, W.U., Yifei, S., Ruifu, Z., Qirong, S., and Qiwei, H. (2014). Investigation of the colonization patterns of plant growth-promoting rhizobacteria *Bacillus amyloliquefaciens* SQR9 on banana roots. J. Nanjing Agric. Univ. *37*, 59–65. https://doi.org/10.7685/j.issn.1000-2030.2014.06.009.

66. Wang, D., Xu, A., Elmerich, C., and Ma, L.Z. (2017). Biofilm formation enables free-living nitrogen-fixing rhizobacteria to fix nitrogen under aerobic conditions. ISME J. *11*, 1602–1613. https://doi.org/10.1038/ismej.2017.30.

67. Ghosh, R., Barman, S., and Mandal, N.C. (2019). Phosphate deficiency induced biofilm formation of *Burkholderia* on insoluble phosphate granules plays a pivotal role for maximum release of soluble phosphate. Sci. Rep. *9*, 5477. https://doi.org/10.1038/s41598-019-41726-9.

68. Mamadou, P., Ndour, S., and Heulin, T. (2020). The rhizosheath : from desert plants adaptation to crop breeding. Plant Soil *456*, 1–13. https://doi.org/10.1007/s11104-020-04700-3.

69. Azulay, D.N., Spaeker, O., Ghrayeb, M., Wilsch-Bräuninger, M., Scoppola, E., Burghammer, M., Zizak, I., Bertinetti, L., Politi, Y., and Chai, L. (2022). Multiscale X-ray study of *Bacillus subtilis* biofilms reveals interlinked structural hierarchy and elemental heterogeneity. Proc. Natl. Acad. Sci. USA *119*, e2118107119. https://doi.org/10.1073/pnas.2118107119.

70. Sathyaseelan, C., Nallusamy, S., Kannusamy, G., Chidambaram, L., Remadevi, R., and Shanmugam, V. (2025). Evolutionary and functional insights into *FRO2* genes in *Oryza sativa*: comparative in silico analysis of iron uptake mechanisms across plant species. Discov. Plants *2*, 37. https://doi.org/10.1007/s44372-025-00087-6.

71. Ishimaru, Y., Suzuki, M., Tsukamoto, T., Suzuki, K., Nakazono, M., Kobayashi, T., Wada, Y., Watanabe, S., Matsuhashi, S., Takahashi, M., et al. (2006). Rice plants take up iron as an Fe^{3+}-phytosiderophore and as Fe^{2+}. Plant J. *45*, 335–346. https://doi.org/10.1111/j.1365-313X.2005.02624.x.

72. Soviguidi, D.R.J., Duan, Z., Pan, B., Lei, R., and Liang, G. (2025). Function, structure, and regulation of Iron Regulated Transporter 1. Plant Physiol. Biochem. *219*, 109457. https://doi.org/10.1016/j.plaphy.2024.109457.

73. Vert, G., Barberon, M., Zelazny, E., Séguéla, M., Briat, J.F., and Curie, C. (2009). Arabidopsis IRT2 cooperates with the high-affinity iron uptake system to maintain iron homeostasis in root epidermal cells. Planta *229*, 1171–1179. https://doi.org/10.1007/s00425-009-0904-8.

74. Robe, K., Stassen, M.J.J., Watanabe, S., Espadas, J., Gonzalez, P., Rossille, A., Li, M., Hem, S., Roux, A., Santoni, V., et al. (2025). Coumarin-facilitated

iron transport: an IRT1 independent strategy for iron acquisition in *Arabidopsis thaliana*. Plant Commun. *6*, 101431. https://doi.org/10.1016/j.xplc.2025.101431.

75. Pii, Y., Penn, A., Terzano, R., Crecchio, C., Mimmo, T., and Cesco, S. (2015). Plant-microorganism-soil interactions influence the Fe availability in the rhizosphere of cucumber plants. Plant Physiol. Biochem. *87*, 45–52. https://doi.org/10.1016/j.plaphy.2014.12.014.
76. Singh, P., Kumar, R., Khan, A., Singh, A., and Srivastava, A. (2023). Bacillibactin siderophore induces iron mobilisation responses inside aerobic rice variety through YSL15 transporter. Rhizosphere *27*, 100724. https://doi.org/10.1016/j.rhisph.2023.100724.
77. Dimopoulou, A., Theologidis, I., Benaki, D., Koukounia, M., Zervakou, A., Tzima, A., Diallinas, G., Hatzinikolaou, D.G., and Skandalis, N. (2021). Direct antibiotic activity of bacillibactin broadens the biocontrol range of *Bacillus amyloliquefaciens* MBI600. mSphere *6*, e0037621. https://doi.org/10.1128/mSphere.00376-21.
78. Jin, C.W., Li, G.X., Yu, X.H., and Zheng, S.J. (2010). Plant Fe status affects the composition of siderophore-secreting microbes in the rhizosphere. Ann. Bot. *105*, 835–841. https://doi.org/10.1093/aob/mcq071.
79. Nithyapriya, S., Lalitha, S., Sayyed, R.Z., Reddy, M.S., Dailin, D.J., El Enshasy, H.A., Luh Suriani, N., and Herlambang, S. (2021). Production, purification, and characterization of bacillibactin siderophore of *Bacillus subtilis* and its application for improvement in plant growth and oil content in sesame. Sustain. Times *13*, 5394. https://doi.org/10.3390/su13105394.
80. Singh, P., Khan, A., Kumar, R., Ojha, K.K., Singh, V.K., and Srivastava, A. (2023). In silico analysis of comparative affinity of phytosiderophore and bacillibactin for iron uptake by YSL15 and YSL18 receptors of *Oryza sativa*. J. Biomol. Struct. Dyn. *41*, 2733–2746. https://doi.org/10.1080/07391102.2022.2037464.
81. Shao, J., Liu, Y., Xie, J., Štefanič, P., Lv, Y., Fan, B., Mandic-Mulec, I., Zhang, R., Shen, Q., and Xu, Z. (2022). Annulment of bacterial antagonism improves plant beneficial activity of a *Bacillus velezensis* consortium. Appl. Environ. Microbiol. *88*, e0024022. https://doi.org/10.1128/aem.00240-22.
82. Yan, W., Qiu, M., Liu, Y., Xue, Y., Tao, L., Xu, Z., Shen, B., Zhang, R., and Shen, Q. (2021). Screening of genes related to kin recognition and discrimination in *Bacillus amyloliquefaciens* SQR9. J. Nanjing Agric. Univ. *41*, 119–126. https://doi.org/10.7685/jnau.202003038.
83. Marquès-Bueno, M.D.M., Morao, A.K., Cayrel, A., Platre, M.P., Barberon, M., Caillieux, E., Colot, V., Jaillais, Y., Roudier, F., and Vert, G. (2016). A versatile multisite gateway–compatible promoter and transgenic line collection for cell type–specific functional genomics in Arabidopsis. Plant J. *85*, 320–333. https://doi.org/10.1111/tpj.13099.
84. Alonso, J.M., Stepanova, A.N., Leisse, T.J., Kim, C.J., Chen, H., Shinn, P., Stevenson, D.K., Zimmerman, J., Barajas, P., Cheuk, R., et al. (2003). Genome-wide insertional mutagenesis of *Arabidopsis thaliana*. Science *301*, 653–657. https://doi.org/10.1126/science.1086391.
85. Arnow, L.E. (1937). Colorimetric determination of the components of 3, 4-dihydroxyphenylalanine-tyrosine mixtures. J. Biol. Chem. *118*, 531–537. https://doi.org/10.1016/s0021-9258(18)74509-2.
86. Riemer, J., Hoepken, H.H., Czerwinska, H., Robinson, S.R., and Dringen, R. (2004). Colorimetric ferrozine-based assay for the quantitation of iron in cultured cells. Anal. Biochem. *331*, 370–375. https://doi.org/10.1016/j.ab.2004.03.049.
87. Wang, T., Wang, N., Lu, Q., Lang, S., Wang, K., Niu, L., Suzuki, M., and Zuo, Y. (2023). The active Fe chelator proline–2'–deoxymugineic acid enhances peanut yield by improving soil Fe availability and plant Fe status. Plant Cell Environ. *46*, 239–250. https://doi.org/10.1111/pce.14459.
88. Love, M.I., Huber, W., and Anders, S. (2014). Moderated estimation of fold change and dispersion for RNA-seq data with DESeq2. Genome Biol. *15*, 1–21. https://doi.org/10.1186/s13059-014-0550-8.
89. Livak, K.J., and Schmittgen, T.D. (2001). Analysis of relative gene expression data using real-time quantitative PCR and the $2^{-\Delta\Delta CT}$ method. Methods *25*, 402–408. https://doi.org/10.1006/meth.2001.1262.

STAR★METHODS

KEY RESOURCES TABLE

REAGENT or RESOURCE	SOURCE	IDENTIFIER
Bacterial and virus strains		
B. velezensis SQR9	CGMCC, China	5808
Bacillus subtilis NCIB3610	Rizzi et al.[50]	N/A
B. velezensis SQR9-*gfp*	Sun et al.[61]	N/A
B. velezensis SQR9-pUBXC	Liu et al.[46]	N/A
Δ*tasA*	Xu et al.[45]	N/A
Δ*feuB*	Xu et al.[45]	N/A
Δ*yusV*	Xu et al.[45]	N/A
Δ*sinI*	Xu et al.[45]	N/A
Δ*spo0A*	Shao et al.[81]	N/A
Δ*sfp*	Shao et al.[81]	N/A
Δ*flhO*	Yan et al.[82]	N/A
Δ*swrC*	Xu et al.[45]	N/A
Δ*hag*	Xu et al.[45]	N/A
Δ*fliD*	Huang et al.[48]	N/A
Δ*dhaS*	Shao et al.[47]	N/A
Δ*yhcX*	Shao et al.[47]	N/A
Δ*ysnE*	Shao et al.[47]	N/A
Δ*yclC*	Shao et al.[47]	N/A
Δ*dhbA*	This study	N/A
Δ*epsD*	This study	N/A
Δ*epsD*Δ*tasA*	This study	N/A
Δ*abrB*Δ*dhbA*	This study	N/A
Δ*sinR*Δ*dhbA*	This study	N/A
Δ*dhbA-gfp*	This study	N/A
Δ*epsD*Δ*tasA-gfp*	This study	N/A
Δ*sinR*Δ*dhbA-gfp*	This study	N/A
Chemicals, peptides, and recombinant proteins		
Chloramphenicol	Sigma-Aldrich	C0378
Erythromycin	Sigma-Aldrich	E5389
Zeocin	Sigma-Aldrich	P9564
Spectinomycin	Sigma-Aldrich	S9007
2,3-Dihydroxybenzoic acid	Sigma-Aldrich	126209
Enterobactin	Sigma-Aldrich	E3910
Ferrozine	Sigma-Aldrich	P9762
^{57}Fe	ISOREAG	21B010-A3
Critical commercial assays		
Plant RNA Kit	Omega Bio-Tek	R6827
HiScript II Q RT SuperMix for qPCR	Vazyme Biotech	R223
ChamQ SYBR Color qPCR Master Mix	Vazyme Biotech	Q411
Bacterial Genomic DNA Kit	Sigma-Aldrich	NA2120
Phanta Max Super-Fidelity DNA Polymerase	Vazyme Biotech	P505
Gel Extraction kit	Omega Bio-Tek	D2500

(*Continued on next page*)

Continued

REAGENT or RESOURCE	SOURCE	IDENTIFIER
Deposited data		
B. velezensis strain SQR9 genome sequence	Zhang et al.[63]	CP006890
Root transcriptomics responses to SQR9 colonization	This study	PRJNA1083752
Experimental models: Organisms/strains		
Arabidopsis: wild type (Col-0)	Li et al.[41]	N/A
Arabidopsis: *IRT1::H2B-2xmCherry*	Marquès-Bueno et al.[83]	N/A
Arabidopsis: *irt1*	Alonso et al.[84]	SALK_097869
Arabidopsis: *fro2*	Alonso et al.[84]	SALK_200098
Oligonucleotides		
Primers are listed in Table S4	This paper	N/A
Recombinant DNA		
Plasmid: pNW33n-*gfp*	Huang et al.[48]	N/A
Software and algorithms		
ImageJ	NIH	https://imagej.nih.gov/ij/
Data Processing System 7.05	Hangzhou RuiFeng Information Technology	http://www.dpsw.cn/
GraphPad Prism 10.1.2	GraphPad Software	https://www.graphpad.com/
Biorender	Biorender	https://app.biorender.com/
Other		
Microplate reader	Molecular Devices	SpectraMax i3x
Chlorophyll meter	Konica Minolta	SPAD-502 Plus
Real-Time PCR System	Applied Biosystems	StepOnePlus
Confocal laser scanning microscope	Leica	TCS SP8
Inductively coupled plasma mass spectrometry	Thermo Scientific	iCAP Q
X-ray fluorescence spectrometer	Bruker	M4 TORNADO

EXPERIMENTAL MODEL AND STUDY PARTICIPANT DETAILS

Strains, culture conditions, and mutant construction

Strains used in this study are listed in Table S3. *B. velezensis* strain SQR9 (China General Microbiology Culture Collection Center, CGMCC accession number 5808; NCBI genome sequence accession number CP006890) and *B. subtilis* NCIB 3610 were used throughout this study. All strains were grown at 30°C in lysogeny broth (LB, 10 g/L tryptone, 5 g/L yeast extract, 5 g/L NaCl). When necessary, final concentrations of antibiotics were added as follows: 20 mg/L zeocin, 5 mg/L chloramphenicol, 100 mg/L spectinomycin, 1 mg/L erythromycin. MSgg medium (5 mmol/L potassium phosphate, 100 mmol/L 3-(N-morpholino) propanesulfonic acid (MOPS), 2 mmol/L $MgCl_2$, 700 μmol/L $CaCl_2$, 50 μmol/L $MnCl_2$, 50 μmol/L $FeCl_3$, 1 μmol/L $ZnCl_2$, 2 μmol/L thiamine, 0.5% glycerol, 0.5% glutamate, 50 μg/mL tryptophan, 50 μg/mL phenylalanine, pH 7.0) was used for biofilm formation. The medium was solidified with 1.5% agar. MKB medium (2.5 g/L $K_2HPO_4{\cdot}3H_2O$, 2.5 g/L $MgSO_4{\cdot}7H_2O$, 15 mL/L glycerin, 5 g/L casamino acids, pH 7.2) was used to detect catecholate siderophore. Fermentation medium (60 g/L cornmeal, 30 g/L soybean meal, 10 g/L glucose, 5 g/L $MgSO_4{\cdot}7H_2O$, 15 g/L $K_2HPO_4{\cdot}3H_2O$, pH 7.0) was used for the large-scale culture of SQR9 in the fermenter. Gene deletion mutants were constructed by an allelic exchange method as described previously.[46] Primers used for PCR in this study are listed in Table S4. The *Escherichia coli-Bacillus* shuttle vector, pNW33n-*gfp*, was introduced into the competent cells of SQR9 mutants to construct GFP-labeled strains.[48]

Plant materials and growth conditions

Arabidopsis thaliana accession Col-0 was used as the wild type in this study. The marker line *IRT1::H2B-2xmCherry*,[83] and the mutant lines *irt1*,[84] and *fro2*,[84] were used in this study. For all experiments, Arabidopsis seeds were surface sterilized with 2% (v/v) NaClO for 10 min and sown on 1/2 Murashige and Skoog (MS) medium with 2% (w/v) sucrose and 1% agar in square Petri dishes (13 × 13 cm). After stratification at 4°C for 2 d, the Petri dishes were positioned vertically and grown under 16 h light and 8 h dark cycles with a light intensity of 100 μmol/m^2/s at 22°C. 1/2 Hoagland medium (5 mmol/L KNO_3, 2 mmol/L $MgSO_4$, 2 mmol/L $Ca(NO_3)_2$, 2.5 mmol/L KH_2PO_4, 70 μmol/L H_3BO_3, 14 μmol/L $MnCl_2$, 1 μmol/L $ZnSO_4$, 0.5 μmol/L $CuSO_4$, 10 μmol/L NaCl, 0.2 μmol/L Na_2MoO_4, 4.7 mmol/L MES, 1% sucrose, pH 5.5) with different concentrations of Fe(III)EDTA was used for plant-bacteria co-cultivation. 1/2 Hoagland medium was solidified with 1% agar.

Pot experiments were conducted in the greenhouse at Nanjing Agricultural University from December 2023 to January 2024. The calcareous soil was collected from a field site located in Suzhou, Anhui Province, China (116.367° E, 34.443° N) and had the following properties: pH 8.1, $CaCO_3$ 361.6 g/kg, organic matter 10.5 g/kg, available *N* 107 mg/kg, available P 13.9 mg/kg, available K 156 mg/kg and available Fe 8.4 mg/kg. Rice (*Oryza sativa* cv. Nipponbare), cucumber (*Cucumis sativus* cv. Jinchun No. 4), and maize (*Zea mays* cv. Zhengdan 958) were cultivated in pot experiments. 12 rice seeds, 3 cucumber seeds and 5 maize seeds were respectively sown in a pot (12 cm × 10 cm × 8 cm) with 0.5 kg of calcareous soil. After germination, 10 rice seedlings, 1 cucumber seedling and 3 maize seedlings with similar growth status were respectively maintained in each pot through thinning. *B. velezensis* SQR9 was cultured for 24 h in LB medium at 30°C and 170 rpm. The cultures were centrifuged at 6000 rpm for 5 min, and cells were re-suspended in 0.3% NaCl to an OD_{600} of 1.0 (approximately 10^8 CFU/mL). The bacterial suspension was further autoclaved at 121°C for 20 min to obtain the heat-killed bacterial suspension. 7-day-old seedlings were inoculated with the bacterial suspension on the soil around each plant root (50 mL/pot). Control pots were treated with an equal volume of the heat-killed bacterial suspension. Hoagland nutrient solution without Fe (50 mL/pot) was used once a week in order to avoid the other nutrient deficiencies. Plants were grown for another 30 days at 30°C with a 16-h light/8-h dark photoperiod. Every treatment included 12 replicates.

Field experiments were conducted at ten sites across five provinces in northern China. The soils at these sites are generally alkaline. Detailed soil physicochemical properties for each site are provided in Table S1. The cultivated areas for the crops ranged from 2 ha to 120 ha (Table S2). Seven crops were included in the field experiments: tomato (*Lycopersicon esculentum* cv. Liger 87-5), cultivated in Tacheng (82°58′ E, 46°12′ N) and Bozhou (82°30′ E, 44°51′ N), Xinjiang; cotton (*Gossypium hirsutum* cv. Xinluzao 84), cultivated in Karamay (84°53′ E, 45°34′ N), Xinjiang; sunflower (*Helianthus annuus* cv. SH363), cultivated in Altay (87°52′ E, 46°41′ N), Xinjiang; baby cabbage (*Brassica pekinensis* cv. Yulinglong), cultivated in Zhangye (100°26′ E, 38°55′ N), Gansu; pepper (*Capsicum annuum* cv. Honggui 218), cultivated in Hengshui (115°40′ E, 37°44′ N), Hebei; wheat (*Triticum aestivum* cv. Xindong 53), cultivated in Yili (81°31′ E, 43°58′ N) and Changji (87°16′ E, 44°00′ N), Xinjiang; wheat (*Triticum aestivum* cv. Jinmai 92), cultivated in Yuncheng (111°00′ E, 35°01′ N), Shanxi; and maize (*Zea mays* cv. Zhengdan 958), cultivated in Tieling (123°43′ E, 42°13′ N), Liaoning. Wheat was cultivated from autumn 2022 through summer 2023, while baby cabbage was cultivated in autumn 2023. The other crops were cultivated from spring to autumn 2023. The large-scale culture of SQR9 was carried out in a 100-ton fermenter for 48 h at 35°C and 160 rpm. The cultures were centrifuged to concentrate cells, followed by spray drying to obtain a solid bacterial powder (approximately 10^9 CFU/g). The spray drying conditions were set as follows: the inlet air temperature of 130°C, and outlet temperature of 80°C. Bacterial powder was dissolved and diluted in water, then irrigated into crop rhizosphere at the seedling stage with the usage of 150 kg/ha. The same amount of water was irrigated as controls. Field experiments were managed according to local conventional tillage, including irrigation, fertilization, and pesticide application. Crop yield was expressed as tonnes per hectare (t/ha). Yield promotion was indicated as yield increase rate relative to control treatment.

METHOD DETAILS

Plant-bacteria co-cultivation

Bacteria were cultured overnight in LB medium at 30°C and 170 rpm. Bacterial cultures were centrifuged at 6000 rpm for 5 min, and cells were washed twice and re-suspended in 10 mmol/L $MgSO_4$ to an OD_{600} of 1.0 (approximately 10^8 CFU/mL) or 0.001. For the co-cultivation on solid culture medium, 7-day-old Arabidopsis seedlings were transferred to Hoagland agar medium (13 cm × 13 cm plate size) and inoculated by applying 2 μL of the bacterial suspension (OD_{600} = 0.001) or 10 mmol/L $MgSO_4$ halfway down each root. For the co-cultivation in liquid culture medium, 7-day-old Arabidopsis seedlings were placed on the medium of bipartite plates (90 mm in diameter). To ensure that only the roots but not sprouts or leaves provided surface for colonization, one chamber of the Petri dish contained 10 mL of water agar to provide physical support for plant shoots, and the other contained 10 mL of Hoagland solution with 10 μL of the bacterial suspension (OD_{600} = 1.0) or 10 mmol/L $MgSO_4$. After inoculation, plates were sealed with Parafilm and incubated in a growth chamber at 22°C. Every treatment included three replicates.

Leaf chlorophyll measurement

Chlorophyll content from Arabidopsis leaf was measured as described previously.[56] In brief, chlorophyll was extracted by adding 1 mL of DMSO per 30 mg of leaf tissue and incubating samples for 45–60 min at 65°C. After cooling to room temperature, the absorbance of the supernatant at 652 nm was measured using a SpectraMax i3x microplate reader (Molecular Devices, USA). Total chlorophyll (mg/g FW) = $OD_{652} \times Volume_{DMSO}/Input_{FW}/34.5$. Every treatment included at least three replicates. Chlorophyll content in the youngest fully expanded leaves of cucumber, rice and maize was measured using an SPAD-502 Plus chlorophyll meter (Konica Minolta, Japan). Every treatment included 12 replicates.

Root colonization assay

Colonization of Arabidopsis roots was performed according to a modified protocol from Sun.[61] In brief, roots were washed three times with 10 mmol/L $MgSO_4$ to remove non-attached cells, then transferred to 2 mL Eppendorf tubes containing 1 mL of 10 mmol/L $MgSO_4$. Cells were detached by sonication at 30% amplitude for 1 min with a 1 s pulse and 1 s pause (ATPIO-1000D, Nanjing Xianou, China). The resulting cell suspension was diluted and plated on LB agar media to determine the number of colony-forming unit (CFU) per mm of root. Every treatment included three replicates.

Biofilm formation assay

The biofilm formation assay was performed as previously described.[61] Strains were cultured overnight in LB medium at 30°C and 170 rpm. Bacterial cultures were centrifuged at 6000 rpm for 5 min, and cells were washed and re-suspended in MSgg medium to an OD_{600} of 1.0. To observe colony biofilm, 2 μL of suspension was spotted on MSgg medium solidified with 1.5% agar. The plates were incubated at 30°C or 37°C for the indicated time. To observe pellicle biofilm, 20 μL of suspension was cultivated in 2 mL of MSgg medium in a microtiter plate well. The microtiter plates were incubated statically at 30°C or 37°C for the indicated time. Every treatment included six replicates.

Arnow assay

The catecholate siderophore in bacterial culture supernatant was measured using the Arnow assay.[85] Briefly, the overnight bacterial cultures were centrifuged at 6000 rpm for 5 min, and cells were washed and re-suspended in 10 mmol/L $MgSO_4$ to an OD_{600} of 1.0. We then transferred 200 μL of the bacterial suspension into 20 mL of MKB medium. After 48-h incubation at 30°C and 170 rpm, the cell-free supernatant was harvested by centrifugation (12000 rpm, 5 min at 4°C) and filtration (using a 0.22 μm filter). Then, 0.5 mL of cell-free supernatant was added to 0.5 mL of 0.5 mol/L HCl and 0.5 mL of reagent containing 10 g each of $NaNO_2$ and $Na_2MoO_4{\cdot}2H_2O$ in 100 mL water. After the formation of the yellow color, 0.5 mL of 1 mol/L NaOH was added, resulting in the generation of the red color. In the presence of catecholate siderophore, this solution has an absorption maximum at 510 nm. 2,3-dihydroxybenzoic acid (DHBA) was used as a standard for catecholate siderophore.

Iron quantification

For the quantification of iron in biofilms, the colony biofilms were collected in 4 mL of 10 mmol/L $MgSO_4$ with pipette tips after incubation at 30°C for the indicated time. Samples were then mildly sonicated as described in the root colonization assay. The resulting cell suspensions were diluted and plated on LB agar medium to determine the cell numbers, then centrifuged at 14000 rpm for 1 min. The supernatants were ready for the quantification of extracellular (biofilm-bound) iron.[33] Cells after centrifugation were washed once with $MgSO_4$ and EDTA (10 mmol/L and 0.1 mol/L), then washed twice with 10 mmol/L $MgSO_4$. Finally, cells were digested with HNO_3 at 65°C for 45 min. The resultant solutions were ready for the quantification of intracellular iron.[50] All samples were analyzed by inductively coupled plasma mass spectrometry (ICP-MS; iCAP Q, Thermo Scientific, USA). Iron concentration was indicated as molar per cell. Every treatment included six replicates.

The levels of extracellular Fe^{2+} and Fe^{3+} in colony biofilm were measured using a ferrozine assay.[86] Every treatment included four replicates. For the quantification of biofilm-bound iron on roots *in situ*, roots were collected after colonization for 7 days and rinsed three times with 10 mmol/L $MgSO_4$ to remove adhered iron, then transferred to 10 mL collection tubes containing 4 mL of 10 mmol/L $MgSO_4$. Samples were sonicated as described in the root colonization assay, then centrifuged at 14000 rpm for 1 min. Root fresh weights were recorded immediately after removing the free surface moisture with filter paper. The supernatants were measured using a ferrozine assay.[86] Iron content was indicated as micrograms per gram of root fresh weight. Every treatment included three replicates.

The active iron in plants was measured as described previously.[87] In brief, plant materials were chopped and mixed with 1 mol/L HCl at a 1:10 ratio (v/v). The mixture was shaken for 5 h at 150 rpm and then filtered with 0.22 μm filter. The iron concentration was measured by ICP-MS (iCAP Q, Thermo Scientific, USA). Every treatment included at least three replicates.

Micro-X-ray fluorescence

Roots and leaves were sampled after co-cultivation for 7 days and washed with deionized water three times, then attached carefully to Kapton tape. The high-resolution distribution of Fe in the samples was analyzed by a micro X-ray fluorescence (μ-XRF) spectrometer (M4 TORNADO, Bruker, Germany). The X-ray tube voltage was 50 kV, and the tube current was 600 μA. Maps were acquired using a 20 μm spot size and 50 μm spot distance with a dwell time of 2 ms per pixel under vacuum. The color scale was adopted to visualize the distribution of Fe in the maps. A brighter color indicated a higher concentration of the element in the maps. The relative Fe content in the samples was indicated as relative fluorescence intensity quantified using ImageJ (v.1.53). Every treatment included three replicates.

^{57}Fe uptake experiment

In order to determine whether the iron in the biofilm might be absorbed by plants, three different experiments were carried out using the ^{57}Fe isotope. ^{57}Fe metal (95%, ISOREAG, China) was dissolved in 1 mol/L HCl in an ultrasonication bath to a final concentration of 1 mg/mL. For the ^{57}Fe uptake from colony biofilms to plants. *B. velezensis* SQR9 was inoculated on MSgg agar with ^{57}Fe and grown at 30°C for 48 h to form the colony biofilms accumulating ^{57}Fe. 7-day-old Arabidopsis seedlings were grown for 10 days in Fe-free Hoagland agar. Four colony biofilms accumulating ^{57}Fe were transferred to each root using sterile pipette tips. After 2 days of treatment, Arabidopsis seedlings were collected for ICP-MS measurement of ^{57}Fe content. For the ^{57}Fe uptake from the colony biofilm matrices to the plants. Biofilm-bound ^{57}Fe was extracted from the colony biofilms accumulating ^{57}Fe with deionized water as described in iron quantification. 7-day-old Arabidopsis seedlings were grown for 10 days in Fe-free Hoagland agar. Arabidopsis seedlings were subsequently transferred to bipartite plates as described in the co-cultivation in liquid culture medium. One chamber of the Petri dish contained water agar, and the other contained Hoagland solution with biofilm-bound ^{57}Fe extracts at a 1:3 ratio (v/v).

After 2 days of treatment, Arabidopsis seedlings were collected for ICP-MS measurement of ^{57}Fe content. For the ^{57}Fe uptake from biofilms on the roots *in situ* to plants. 7-day-old Arabidopsis seedlings were colonized by *B. velezensis* SQR9 for 7 days in Hoagland with ^{57}Fe as described in the co-cultivation in liquid culture medium. Subsequently, the previously colonized Arabidopsis seedlings were carefully washed with deionized water to remove non-colonizing cells and iron contamination from the medium. Arabidopsis seedlings with *B. velezensis* SQR9 pre-colonization were transferred to bipartite plates as described in the co-cultivation in liquid culture medium. One chamber of the Petri dish contained water agar, and the other contained Fe-free Hoagland solution. Plant shoots were collected for ICP-MS measurement of ^{57}Fe content after 0 and 2 days of transfer. All samples were soaked in 5 mmol/L $CaSO_4$ and 10 mmol/L EDTA mixed solution for 5 min and then rinsed with deionized water three times to remove surface adhered Fe before ICP-MS measurement. Every treatment included three replicates.

RNA sequencing

After co-cultivation for 5 days, Arabidopsis roots were carefully collected in liquid nitrogen, and the total RNA was extracted using the Plant RNA Kit (R6827, Omega Bio-Tek, USA) according to the manufacturer's protocol. RNA quality was assessed on an Agilent 2100 Bioanalyzer (Agilent Technologies, Palo Alto, USA). The cDNA library was sequenced using Illumina Novaseq 6000 by Gene *Denovo* Biotechnology Co. (Guangzhou, China). Clean reads were filtered by Fastp (version 0.18.0) and mapped to the reference genome using HISAT 2.2.4. RNA-Seq data were normalized to FPKM (fragment per kilobase of transcript per million mapped reads). RNA sequencing data were deposited in the NCBI Sequence Read Archive (SRA) with the accession number PRJNA1083752. RNA differential expression analysis was performed by DESeq2 software between two different groups.[88] The genes with the parameter of false discovery rate (FDR) below 0.05 and absolute fold change >2 were considered differentially expressed genes (DEGs).

RT–qPCR

To measure the effect of *B. velezensis* SQR9 colonization on the expression of Fe acquisition-related genes, Arabidopsis roots were carefully collected in liquid nitrogen after co-cultivation for 5 days. To measure the effect of siderophores on the expression of Fe acquisition-related genes, 7-day-old Arabidopsis seedlings were grown in Hoagland solution with or without 10 μmol/L siderophores. After treatment for 24 h, Arabidopsis roots were carefully collected in liquid nitrogen. Total RNA was extracted using the Plant RNA Kit (R6827, Omega Bio-Tek, USA). 500 ng of total RNA was reversely transcribed into cDNA by the HiScript II Q RT SuperMix kit (Vazyme Biotech, China). RT-qPCR was performed on a StepOnePlus Real-Time PCR System (Applied Biosystems, USA) using ChamQ SYBR qPCR Master Mix (Vazyme Biotech, China). The PCR program was as follows: cDNA was denatured for 30 s at 95°C, followed by 40 cycles of denaturation at 95°C for 10 s, and annealing at 60°C for 30 s. *PP2AA3* (At1g13320) was used as the reference gene. The primers were provided in Table S4. The $2^{-\Delta\Delta Ct}$ method was used to analyze the real-time PCR data.[89] Every treatment included four replicates.

Ferric chelate reductase activity

Ferric chelate reductase (FCR) activity was examined as described previously.[17] Roots were washed with deionized water three times, then incubated in the assay solution containing 0.1 mmol/L Fe(III)EDTA and 0.3 mmol/L ferrozine in the dark for 1 h. The absorbance of the assay solutions was recorded at 562 nm. Reduction rates were determined by the formation of the complex Fe(II)-ferrozine based on an extinction coefficient of 28.6 mmol/L/cm. Every treatment included four replicates.

Visualization and quantification of fluorescent phenolic compounds

Hoagland solution was collected after co-cultivation for 5 days and centrifuged at 14000 rpm for 1 min 200 μL of the supernatant was transferred into a 96-well microplate. Fluorescent phenolic compounds were observed after excitation with 365-nm UV light. Fluorescent phenolic compounds (excitation at 360 nm; emission at 528 nm) were measured using a SpectraMax i3x microplate reader (Molecular Devices, USA).[20] Every treatment included six replicates.

Confocal laser scanning microscopy

To observe the colonization of *B. velezensis* SQR9-*gfp* and the expression of *IRT1::H2B-2xmCherry*, roots were sampled and washed gently with deionized water three times, then observed using a confocal laser scanning microscope (TCS SP8; Leica, Germany). The excitation/emission wavelengths were 488 nm/507 nm for GFP, and 587 nm/610 nm for mCherry. Quantification of fluorescence intensities was analyzed using ImageJ (v.1.53). Every treatment included four replicates.

QUANTIFICATION AND STATISTICAL ANALYSIS

Each experiment was performed at least three times. Data are presented as mean ± standard deviation (SD). Significant differences between treatments were analyzed by Student's *t* test or one-way analysis of variance (ANOVA) followed by Duncan's multiple range test ($p < 0.05$) using the Data Processing System 7.05 (Hangzhou RuiFeng Information Technology Co., Ltd., China). Detailed statistical analyses were described in the figure legends. Plotting was performed with GraphPad Prism 10.1.2 (GraphPad Software, USA).